Curriculum Vitae (C.V.)

ERIN N WILDERMUTH
Email: ewildermuth@gmail.com

EDUCATION

University of Maryland PhD: Spring 2024
Baltimore, MD: Molecular Medicine

London School of Economics MSc: June 2009
London, UK: MSc in Political Economy

American University BA: June 2007
Washington, DC: BA in International Relations

RESEARCH EXPERIENCE

University of Maryland Aug 2018 – March 2024
Medical Scientist Training Program Student, Baltimore, MD

- Created a single-nucleus transcriptomic atlas of a mouse model of alcohol use disorder using bioinformatics skills including original programming in R and mastery of several pipelines involving the use of Seurat, Signac, EdgeR, and related packages.
- Created a single-nucleus transcriptomic atlas of a six-month-old mouse model of Huntington's Disease with a disease-causing CAG repeat length of 111, demonstrating that variability between spiny projection neurons is not yet apparent.
- Used the Huntington's Disease atlas to test the efficacy of an Htt-lowering, non-allele specific antisense oligonucleotide gene therapy product, demonstrating a surprising exacerbation of the HD signature.
- Cell culture involving several human stem cell lines modeling Huntington's Disease

University of Miami Oct 2017 – May 2018
Research Associate, Miami, FL

- Screening FDA-approved drugs on primary cancer cell lines derived from patients to identify candidate compounds for use in personalized medicine under the mentorship of Dr. Shaun P. Brothers of the Center for Therapeutic Innovation.
- High-throughput compound screening.
- Cell culture and cell survival assays with a variety of primary human cell lines.

Icagen Inc. April 2017 – July 2017
Research and Development Intern, Tucson, AZ

- Researched, modified and executed cellular assays with the aim to find compounds that impacted the STING-dependent pathway of interferon-beta production in cells under the mentorship of Dr. Christopher Penton.
- Culture of human cell lines, including THP-1, HEK 293 and Huh7.
- Generation of stable cell lines including siRNA knockdowns and transgenes.
- Immunostaining in 96 well format / high-content imaging via a bioluminescent LumiKine-based ELISA assay to test the impact of compounds on interferon-beta production in cells.
- Designed and implemented counter-screens to test whether alternative, non-STING pathways were contributing to changes in interferon-beta production.

The Brain Institute Aug 2016 – Dec 2016
Research Volunteer, Tucson, AZ

- Contributed to the Barnes' lab Cognitive Aptitude Study in which rats are run through a battery of cognitive assays to identify high performers, medium performers, and low performers in different age groups to help researchers understand how the brain ages over time, and how this process impacts memory and cognitive ability. I was involved in rodent health checks, the handling of new rats, and ran countless animals through several behavioral tests, including the water maze and novel object recognition tests.
- Trained in the Madhavan lab to use a microtome to cut slices of rat brains into wells, correctly ordering stained rat brains from the wells, and mounting them on slides.

SKILLS AND INTERESTS

- Bioinformatics in R, single-cell transcriptomics, Premiere Pro, Final Cut Pro, Photoshop, InDesign, Word, and Excel
- Avid scuba diver (Divemaster)

Abstract

Title of Dissertation: Cell-type specific transcriptomic dysregulation in the striatum are a feature of substance use and neurodegeneration that can be used to evaluate preclinical gene therapy

Erin Wildermuth, Doctor of Philosophy, 2024

Dissertation Directed By: Dr. Seth Ament, Associate Professor, Institute for Genome Sciences; Associate Professor, Maryland Psychiatric Research Center

Alcohol use disorder (AUD) and Huntington Disease (HD) are neuropsychological diseases with an impact on the striatum. AUD is characterized by inflexible drinking, which is thought to be mediated by effects of chronic intermittent ethanol exposure on the dorsal striatum, the input nucleus of the basal ganglia. In our study of AUD, we used single-nuclei RNA-sequencing (snRNA-seq; n = 86,715 cells) to examine the impact of chronic intermittent ethanol exposure on the dorsal striatum in C57BL/6 male and female mice. We detected 462 differentially expressed genes at FDR < 0.05, the majority of which were mapped to spiny projection neurons (SPNs), the most prominent cell type in the striatum. Gene co-expression network analysis and functional annotation of differentially expressed genes revealed down-regulation of postsynaptic intracellular signaling cascades specifically in canonical SPNs. Inflammation-related genes were down-regulated across many striatal cell types. Gene set enrichment analyses also pointed to altered states of rare cell types, including the induction of angiogenesis-related genes in vascular cells. These data provide important clues as to the impact of ethanol on striatal biology and provide a key resource for future investigation.

As a monogenic disorder, Huntington's disease (HD) is at the forefront for gene-therapy innovation in neurodegeneration. One challenge to clinical innovation is our ability to discern detailed information about how HD and its potential therapeutics impact the brain. Single-nucleus RNA sequencing is a cutting-edge technology capable of providing this level of detail. Here, we studied cell type-specific transcriptomic effects of HD mutations in the striatum of a knock-in mouse model, HttQ111/+. Further, we examined the cellular impacts of a non-allele specific Htt-lowering antisense oligonucleotide (ASO). We characterized substantial transcriptional effects of the HD mutation in spiny projection neurons, the cell type most vulnerable to HD neurodegeneration. Surprisingly, Htt-lowering ASO treatment exacerbated many of these transcriptional changes. Understanding these cell type-specific effects of ASO treatment could aid in the interpretation of Htt-lowering toxicity that has recently been observed in human patients

Cell-type specific transcriptomic dysregulation in the striatum are a feature of substance use and neurodegeneration that can be used to evaluate preclinical gene therapy

by

Erin Wildermuth

Dissertation submitted to the Faculty of the Graduate School of the
University of Maryland, Baltimore in partial fulfillment
of the requirements for the degree of
Doctor of Philosophy
2024

Table of Contents

List of Figures

INTRODUCTION

A. The Striatum

The striatum is the major input center of the basal ganglia. Structurally, the ventral striatum is comprised of the nucleus accumbens, implicated in reward circuitry, and the olfactory tubercle. The dorsal striatum is comprised of the caudate nucleus and putamen separated by a white matter tract called the internal capsule. The caudate nucleus and putamen play complementary functional roles, with the dorsal striatum often viewed as a whole involved in executive functioning, motor regulation, cognition, learning and habit formation. When relevant, further compartmentalization is typically made between dorsomedial and dorsolateral striatum, which are associated with goal-directed learning and habit formation via stimulus-response processes respectively.[1]

Striatal Circuits

Major inputs to the striatum include thalamic and cortical excitatory glutaminergic projections modulated by dopaminergic projections from the substantia nigra pars compacta (SNc) and ventral tegmental area (VTA) midbrain dopaminergic neurons.[2]

Outputs from the striatum are filtered from inputs and funneled through two distinct pathways, known as the “Direct” striatonigral pathway and “Indirect” striatopallidal pathway. These paths are regulated by two distinct populations of Spiny Projection Neurons (SPNs), GABAergic neurons that make up roughly 95% percent of the cell population of the striatum. Direct Spiny Projection Neurons (dSPNs) are associated with the “Direct” pathway and express high levels of the D1 dopamine receptor. This pathway involves inhibitory output to the internal globus pallidus (GPi) and substantia nigra pars

reticulata (SNr) resulting in disinhibition of the thalamocortical and brainstem motor circuits. In our most simplistic models, dSPNs are considered an on-switch. Indirect Spiny Projection Neurons (iSPNs) are associated with the "Indirect" pathway and express high levels of the D2 dopamine receptor. These cells direct output to the external globus pallidus (GPe) and subthalamic nucleus (STN) resulting in inhibition of thalamocortical circuitry and movement – the off-switch. These two pathways and the associated roles dSPNs and iSPNs are projected to play represent an overly simplistic delineation of circuitry and how cell-type specificity regulates striatal function, which is further discussed below as related to AUD and HD.

Striatal Cell Types

This striatum is endowed with a rich diversity of cell types. GABAergic Spiny projection neurons (SPNs) make up 95% of the striatal neuronal population and are canonically compartmentalized into direct (dSPN) and indirect (iSPN) types.[3] As outlined above, dSPNs express the D1 dopamine (DA) receptor and primarily stimulate action via the direct pathway. iSPNs express the D2 DA receptor with activation reinforcing inaction via the indirect pathway. Many studies attempt to further subdivide SPN populations, an indication that these striatal residents are more heterogeneous than scholars originally surmised. The most pronounced and distinct population of SPNs aside from canonical dSPN and iSPN are defined by the expression of *Otof*+ alongside mixed markers predominantly expressed by dSPNs and iSPNs. The third subcluster is termed "eccentric" (eSPN).[4–6] Our understanding of the functional annotation of eSPNs is limited.

Interneurons (INs), which project locally and modulate striatal outputs, also populate the striatum. Three key subtypes include GABAergic somatostatin-expressing (*SST*+) INs,

GABAergic parvalbumin-expressing (*PV+*) INs, and cholinergic acetyltransferase-expressing (*ChAT+*) INs. SST-INs are low-threshold spiking (LTS) cells with stretched axons and broadly branched dendrites suggestive of distant target capacity.[7,8] SST-INs primarily transmit GABA, while co-expressing SST, neuropeptide-Y (NYP) and nitric oxide (NO).[9–11] Paradoxically, the excitatory neurotransmitter glutamine is also co-expressed by SST-INs, allowing for both inhibitory and excitatory transmission to post-synaptic targets.[12] PV-INs are fast-spiking interneurons (FSIs) known to transmit both to SPNs and to other FSIs.[13] They are morphologically spherical with dendrites exhibiting comparatively little branching and highly compact, densely-branched axons best suited to local transmission.[13] PV-INs provide feed-forward inhibition on SPNs, though this action may be modulated by FSI-FSI innervations.[14,15] CHAT-INs are large aspiny interneurons that project widely throughout the striatum. Current estimates of axonal varicosities per cell average 500,000.[16] Acetylcholine plays diverse roles in the striatum, with modulation resulting in varied and significant downstream effects that are poorly characterized but likely to influence striatal output.[16] As the primary source of acetylcholine in the striatum, CHAT-INs hold significance beyond their small population size.[16]

The other resident cells of the striatum are more common neuronal cell types including astrocytes, oligodendrocytes, polydendrocytes, endothelial cells, mural cells, ependymal cells, and microglia. Though most of these cell type do not have known striatal-specific attributes, striatal astrocytes are distinct in their comparatively low expression of the common astrocyte marker gene glial fibrillary acid protein (*Gfap*).[17] When compared to hippocampal astrocytes, striatal counterparts display robust potassium-channel expression and are also enriched for proteins involved in calcium flux and binding.[17] Astrocytes are

believed to directly contact approximately eleven SPNs and play a role in neuromodulation.[17]

B. Alcohol Use Disorder

Addiction is a devastating condition that impacts a large percentage of the U.S. population and carries grave social, healthy, and economic costs. Alcohol Use Disorder (AUD) is a mental health condition characterized by compulsive heavy intake of alcohol, often following a chronic, relapsing pattern over many years. AUD affects >5% of the global population and is associated with enormous medical and economic consequences, including ~140,000 annual deaths from alcohol-related causes in the United States alone.[18] One-third of Americans will meet the criteria for AUD during the course of their lifetimes.[19] Only a small proportion of people living with AUD are adequately treated by existing therapies. The development of more effective therapies has been hindered by incomplete understanding of alcohol's effects on the brain. The neurobiology of AUD closely mirrors that of other disorders of addiction.

Addiction is a three-stage cycle of progressive repetition involving intoxication, withdrawal, and anticipation, all of which play a role in dysregulating reward circuits to encourage obsessive, habit-based behaviors.[20] Decision-making shifts from executive-function-based (prefrontal cortex) to habit-based (striatum), accompanied by a progression from ventral to dorsal striatal predominance.[21]

Activation of the reward system is predicated by increased dopamine and opioid peptide release into the ventral striatum from ventral tegmental area (VTA) midbrain dopaminergic neurons, which activates D1 receptors causing the intoxicating feelings

experienced in the first stage of an addictive cycle. At the same time, increased dopamine release into the dorsal striatum is associated with goal-directed learning and habit formation.[22] These core events set in motion a complicated range of neurotransmitter dysregulation that ultimately uses the brain's natural capacity for neuroplasticity to change important circuitry.

Both dorsolateral and dorsomedial compartments of the striatum are involved in addiction circuitry, with the dorsolateral striatum implicated in habit formation via stimulus-response processes and the dorsomedial striatum implicated in goal-directed learning and behaviors. Progression from ventral to dorsal striatal predominance in addiction may be bolstered by inter-striatal loops innervating the dorsal striatum via dopaminergic neurons of the brainstem.[23]

The neuronal cellular residents of the dorsal striatum are representative of the striatum as a whole with roughly 95% SPNs and 5 percent interneurons (iNs). The roles played by iSPNs as compared to dSPNs in addiction are poorly understood. There is some consensus that, as per dogma, dSPNs are likely to stimulate action while iSPN activation reinforces inaction, but studies indicate that this stratification of roles is overly simplistic.[22] Research focusing on SPN activity have shown activation of iSPNs alongside dSPNs during action promotion and the two cell types exhibit different patterns of activation depending on the activity initiated.[22]

The Striatum in AUD

The dorsal striatum is a key structure dysregulated in humans with AUD, as well as in animal models of chronic alcohol intake.[20] Alcohol, like other addictive substances, causes dopamine and opioid peptides to be released into the both the dorsal and ventral striatum from midbrain dopaminergic neurons and subsequent activation of striatal neurons. The activation of ventral striatum contributes to the hedonic, intoxicating effects of alcohol intake. Dorsal striatum activation is associated with goal-directed learning and habit formation.[22] Chronic alcohol use also impacts circuits involved in memory and learning, key process controlled by the striatum.[24]

At a cellular level, chronic alcohol intake is associated with well-described anatomical and functional changes in spiny projection neurons (SPNs), the GABAergic output neurons of the striatum. Biochemical studies of the striatum indicate specific attenuation of the indirect pathway in chronic alcohol exposure.[25] Further, chemogenic inhibition of the direct path ameliorates cue-induced drug seeking in rats.[26] However, the molecular adaptations contributing to these alcohol-induced changes remain poorly characterized. Major effects include those that influence (1) glutamate synapses (2) morphological and intrinsic excitability, and (3) GABA synapses. Glutamate is the major excitatory neurotransmitter in the brain. Ethanol has been shown to increase activity in NR-2B containing NMDA receptors and AMPA receptors in the dorsal striatum of rats.[27–29] Other studies point to a dose-dependent decrease in excitatory postsynaptic currents, suggesting an inhibition of glutaminergic synaptic transmission.[30] Glutaminergic projections originating from the anterior insular cortex have been implicated in particular, with evidence that synaptic plasticity at this junction is particularly vulnerable to ethanol

exposure.[31] Morphologically, chronic ethanol exposure has been shown to induce dendritic hypertrophy, increasing dendritic length and branch count in the dorsal striatum.[32] These structural changes are mirrored by functional changes including loss of synaptic plasticity.[32–34] BDNF signaling, corticosteroids, and stress have been identified as a potential source of self-administration gating.[35,36] Intrinsic excitability is also altered in complex and cell-type specific ways.[37] Ethanol exposure causes reduced GABAergic transmission onto SPNs, with subsequent disinhibition of the dorsal striatum. The activation of delta opioid receptors and potentiation of GABAergic input to fast-spiking interneurons may contribute to this phenomenon.[38,39] Understanding the nature of these diverse effects and the cellular sources of the expression changes driving these effects is required.

The Use of Animal Models in Addiction

The study of addiction has been aided immensely by the use of animal models, especially rodents. Two forms of experimental design common in the literature are intermittent exposure, where animals are exposed to the substance independent of their actions, and behavior-oriented designs that allow animals access and control over substance use. Each carries its own limitations with exposure allowing for subjects who have been exposed to equal levels of addictive substances and behavioral-based studies better mirroring human addiction in terms of reward-seeking behavior emulation. In this study we use the C57BL/6 J mouse model, a verified mouse model commonly used in alcohol use disorder studies, under an intermittent exposure design paradigm.

Genomic Studies in AUD

Single-cell genomics has emerged as a powerful strategy to describe the cell type-specific molecular adaptations associated with exposure to addictive substances.[40,41] Only a few single-cell genomics studies have described changes in AUD or AUD-related animal models, primarily on the prefrontal cortex.[42–45] Genomic profiling of the striatum in AUD and related models has been limited to snRNA-seq of the ventral striatum in a small cohort of human AUD cases and controls, which was underpowered to detect many differentially expressed genes. RNA sequencing of bulk tissue from larger cohorts found significant dysregulation of immune and inflammatory processes.[46]

C. Huntington's Disease

As modern medicine allows people to live longer, age-related cognitive decline and neurodegeneration is becoming an increasingly urgent problem. Neurodegenerative diseases are among the leading causes of death and disability in the United States. Neurodegenerative disease, particularly Alzheimer's disease (AD), is the leading cause of dementia, an umbrella term referring to a state of mind involving challenges with memory, problem solving, and other cognitive activities that impact everyday life. AD is the most widespread of the dementia-causing diseases with 1.5 percent of the US population suffered from AD and related dementia in 2014 and 3.3 percent projected to be affected by 1960 as our population ages.[47]

Huntington's disease (HD) is the most common monogenic neurodegenerative disease, impacting ~1 in 10,000, and represents an excellent model for understanding molecular and cellular mechanisms of neurodegeneration. HD is caused by a trinucleotide CAG

repeat on exon 1 of the HTT gene and results in a mutant huntingtin protein containing a polyglutamate tract. Age of onset depends on several factors including the length of the CAG repeat, which increases generationally. Greater than 60 repeats is associated with juvenile onset while 40-50 repeats tracks to adult onset. While CAG repeat number explains roughly 66% of HD variance other inputs, both environmental and genetic, are likely to play a role.[48,49] HD has its own set of unique clinical features that distinguish it from other forms of neurodegeneration and from age-related cognitive decline when taken together, but each case of HD is unique and signs can differ between patients.[50] The clinical manifestation of HD include motor, cognitive and psychiatric dysfunction. Chorea, characterized by involuntary sudden movements, is a common symptom of HD but the progression of movement dysregulation is more complicated and often follows a biphasic pattern that begins with hyperkinesis and progresses into hypokinesis.[51] Though motor symptoms are often the most identifiable symptoms of HD, cognitive and psychiatric dysfunction can begin fifteen years earlier and reportedly make up a greater percentage of disease burden for HD patients and their families.[52] As such there has been an increased interest in the study of prodrome manifestations of HD, including cognition and psychiatric affects.[52] Our study complements this shift by examining striatal dysregulation and rescue in early disease.

Cells in HD exhibit signs of accelerated aging.[53] This raises the question of whether HD, as a monogenic disease, can shed light on the underlying mechanisms that cause age related cognitive decline and susceptibility to other neurodegenerative diseases. This possibility is bolstered by an increased vulnerability to other neurodegenerative diseases in HD patients – one study found that 82% (9 of 11) deceased HD patients with a mean

age of 76 showed evidence of AD pathology while only 16% of aged people 76-84 years in the general population would be expected to show signs of disease.[54,55] Further studies have found wider evidence of neurodegenerative co-pathies in HD, with 88% of deceased HD patients exhibiting pathological evidence of other disease compared to 29% of controls.[56]

The Striatum in Huntington's Disease

Regional degeneration is one of the factors used to distinguish different forms of neurodegenerative disease and primary degeneration of the striatum is a key feature of HD, with iSPNs being affected earlier and more severely than dSPNs. Biphasic motor manifestations of HD mirror the neurobiological vulnerability patterns of SPNs – with hyperkinesis occurring earlier as iSPNs are selectively damaged, followed by hypokinesis with loss of dSPNs in later stages of disease.[51] Cognitive and psychiatric symptoms are also likely to be associated with striatal dysregulation. In addition to the timing of striatal degeneration most closely matching prodromal HD symptoms, cortical-striatal pathways link the prefrontal cortex to the dorsal striatum and lesion studies based in monkeys and rats have shown that lesions in the dorsal striatum can affect cognition and executive function similarly to prefrontal lesions.[57]

The Use of Animal Models in HD

Though HD occurs only in humans, the use of animal models is essential in allowing experiments and manipulations that are not possible in a human population. Mice with varying CAG repeat lengths are a verified and highly documented model for HD.[49,58–60] CAG knock-in lengths that would result in disease features in humans (i.e. 40-50) do not

result in HD-associated phenotype in knock-in mouse models, with a phenotype arising in lengths greater than 90 repeats.[60] HD model mice exhibit a range of relevant behavioral and molecular characteristics. Behavior and motor deficits, including deficits in gait, have been documented in the CAG 140 knock-in mouse model.[61–63] Q111 is a mouse model with a knock-in CAG repeat of 111. This model produces similar results on several genetic backgrounds, with disease-associated characteristics progressing more rapidly on the B6 mouse background.[49] Though most HD studies center on older mice, the striatum of the B6-Q111 mouse model has been experimentally evaluated at younger time points with evidence of (1) fewer than 25 DEGs at the 4-9 week window, (2) 279 DEGs at the 9-16 week window, and (3) 1513 DEGs at the 16-20 week window.[49]

Genomic Studies in Striatal HD

HD is a widely studied neurodegenerative disease with a strong library of literature. The HD molecular signature has previously been studied in bulk RNA-seq.[64] The seminal bulk RNA-seq study, conducted by Langfelder et. al., studied over 400 striatal samples from HD knock-in mice across several CAG repeat lengths including Q20, Q80, Q92, Q111, Q140, and Q175, and three age groups including 2 months, 6 months, and 10 months. When compared to WT animals, striatal tissues revealed significant age and CAG repeat length dependent transcriptional changes. Network analysis revealed 13 significantly differentially expressed striatal modules. Modules negatively correlated with CAG repeat lengths included modules biologically associated with (1) cAMP signaling and striatal marker genes), (2) glia, (3) glutamate receptor signaling, and (4) transcription and chromatin factors. Modules positively correlated with CAG repeat lengths include modules biologically associated with (1) cell division and protocadherin genes, (2) stress

response genes, (3) mitochondrial genes, and (4) protein homeostasis genes. Major take-aways from the paper included CAG length dependent of dysregulation in striatal SPN cell-identity genes, and upregulation of genes involved in cell death signaling.

Studies in single cell are more limited. A 2020 paper employed the translating ribosome affinity purification (TRAP) methodology to examine cell-type specific gene expression across knock-in mouse model at differing CAG lengths and with a transgenic HD mouse model.[65] Results showed downregulation of striatal identity genes in both iSPNs and dSPNs alongside dysregulation of circadian clock and synaptic genes. Other results common between canonical SPNs include upregulation of DNA mismatch repair pathway, widely believed to contribute to CAG repeat instability, and downregulation of the BDNF receptor *Ntrk2*. An interesting cell-type specific change in iSPNs was downregulation of the OXPHOS pathways, a finding the authors posited may be related to the cell type's particular vulnerability in HD. They further found evidence of iSPN mtRNA release at an early timepoint (3m) accompanied by activation of the innate immune system.

Malaiya et. al. analyzed 14-15-month-old Q175 HD model mice at the single cell level using RNA-seq.[66] Results from this study built upon previous literature, finding striatal cell identify dysregulation to exist in a bidirectional manner across cell types, with downregulation of the cell type specific genes that should have identified a particular cell and upregulated of other cell type specific genes. This was posited as a potential effect of PCR2 dysregulation. Other findings from the study include (1) increased microglia in striatal HD (2) a disease-specific neuroinflammatory signature across several cell types, and (3) thousands of dysregulated genes in glia, especially in oligodendrocytes and

astrocytes, which appear to show a time trajectory of dysregulation as opposed to distinct results between WT and HD. These studies highlight the importance of exploring transcriptional dysregulation at the single-cell level.

D. Associations between Alcohol Use Disorder and Neurodegenerative Disease

AUD is thought to exacerbate neurodegenerative disease through several key pathways, notably including oxidative stress, proteinopathy, inflammation, and induction of the stress response.[67] Evidence from the National Research Roster on HD indicates that alcohol and nicotine use are associated with greater evidence of psychiatric disease in HD as well as an earlier age of onset.[68] Continued alcohol use was also found to be associated with faster progression of psychiatric symptoms.[68] A more recent study based on Enroll-HD global platform data also finds an increased progression in psychiatric symptoms with increased alcohol use in HD.[69] This study further notes an increased progression in motor symptoms, though they did not find a significant relationship between alcohol misuse and the age of HD onset.[69] Proposed parallel pathways involved in AUD and neurodegeneration provide support for a study looking more deeply at the single-cell based molecular underpinnings of these diseases in tandem, especially when taken into consideration alongside clinical associations between AUD and HD.

E. Single Cell Analysis in Therapeutic Development

The computational biology and bioinformatics techniques developing in parallel with our access to increasingly sophisticated biological data have the potential to transform biological research. Diseases that were previously thought to be homogenous are now understood to be molecularly heterogeneous.[70] At the same time, we are finding

similarities between diseases that were thought to be distinct. An increased understanding of the particular molecular interactions that can cause disease, assays that test for these interactions in disease, and therapies that are aimed toward specific genetic and transcriptomic irregularities instead of assuming that similar clinical states are related while dissimilar clinical states are not has the potential to revolutionize medicine; this approach is being used in the field of cancer today to great success.[70] Broadening our application of this approach while harnessing the power of multi-omics in other fields may result in the same paradigm-shifting changes in scientific knowledge that we are witnessing in cancer research.

Single-cell multi-omics techniques are a relatively new and particularly robust scientific assay capable of providing data that allows insights into cell-type specific regulatory and network patterns within healthy individuals and different disease states. In bulk genomic data our understanding of gene networks is limited to those derived from all cell-types together. This is highly limiting both in terms of understanding underlying biology and in developing targeted therapeutics aimed at a specific cell-type. A therapeutic for one cell-type may cause dysregulation in another if applied globally, but we could not predict this without cell-type specific data. This study uses gene regulatory networks to elucidate cell-type specific striatal dysregulation in AUD and to test a proof-of-concept therapy in HD, elucidating ways in which an understanding of gene regulatory networks can be used to identify target genes and develop therapeutics.

One goal in better understanding gene networks is to support the development of targeted gene therapy products that can potentially alter the course of a disease. Not only can advanced single-cell genomics elucidate pathways and potential gene therapy targets, but

these techniques can also support the testing of successful gene therapy ideas. If a developed therapy is meant to lessen or irradicate network-specific transcriptional dysregulation within a specific cell-type, comparison of the model with and without treatment can shed light on whether the treatment is working as expected. Though there are several gene therapy strategies, this proposal includes an assessment of an antisense oligonucleotide therapy (ASO). There are no approved gene therapies in either AUD or HD at this time.

As a monogenic neurodegenerative disease, HD is a prime candidate for gene therapy. Several gene therapy products are at various stages of development for HD, which currently features no disease altering therapies. ASOs, short nucleotides that bind cellular RNA to change their dynamics, are a promising gene therapy option. ASOs can be used to degenerate RNA before transcription, alter splicing patters in pre-RNA or to change RNA-protein interactions. As they depend on complementary base pairing for binding, ASOs can be formulated to target specific RNA transcript and thus limit off-target effects. ASO therapies have seen some success in neurological disease with Nusinersen, an ASO therapy for Spinal Muscular Atrophy, becoming the first neurodevelopmental gene therapy treatment to gain FDA approval in 2016. [71] Unfortunately, a promising ASO treatment for HD, Tominersen, was halted in clinical trials in 2021 due to safety concerns, though work along these lines continues.[72] A post-doc exploratory analysis from the trial indicated that the subgroup of enrolled participants in the 16-week injection group (as opposed to the 8-week injection group) with both a lower age and lower CAP score may have benefited from treatment when compared to controls.[73] Gene therapy in HD is complicated by the biological necessity of wild-type HTT (wtHTT).

Discontinuation of the drug's clinical trial has led some to speculate that an earlier intervention (e.g., in premanifest carriers of the HD mutation) is needed, while others speculate that alternative gene therapies, such as allele specific ASOs that target only the mutant allele are the only way forward. The ASO used in this study will test the first of these possibilities, using an ASO with similar characteristics to Tominersen but with treatment initiated before the onset of disease-relevant phenotypes. Here we will evaluate whether transcriptomic dysregulation of striatal gene networks in an HD mouse model can be rescued using an HTT-lowering gene therapy.

CHAPTER II. A SINGLE-CELL GENOMIC ATLAS FOR THE EFFECTS OF CHRONIC ETHANOL EXPOSURE IN THE DORSAL STRIATUM

A. Abstract

Alcohol use disorder (AUD) is characterized by inflexible drinking, which is thought to be mediated by effects of chronic intermittent ethanol exposure on the dorsal striatum, the input nucleus of the basal ganglia. Despite significant efforts to understand the impact of ethanol on the dorsal striatum, the rich diversity of striatal cell types and multitude of ethanol targets expressed by them necessitates an unbiased, discovery-based approach. In this study, we used single-nuclei RNA-sequencing (snRNA-seq; n = 86,715 cells) to examine the impact of chronic intermittent ethanol exposure on the dorsal striatum in C57BL/6 male and female mice. We detected 462 differentially expressed genes at FDR < 0.05, the majority of which were mapped to spiny projection neurons (SPNs), the most prominent cell type in the striatum. Gene co-expression network analysis and functional annotation of differentially expressed genes revealed down-regulation of postsynaptic intracellular signaling cascades specifically in canonical SPNs. Inflammation-related genes were down-regulated across many striatal cell types. Gene set enrichment analyses also pointed to altered states of rare cell types, including the induction of angiogenesis-related genes in vascular cells. Down-regulation of a gene network enriched for calcium-signaling genes and components of glutamatergic synapses was reproducible in the dorsal striatum of humans with AUD. Genetic perturbations of four of this module's hub genes – *Foxp1*, *Bcl11b*, *Pde10a*, and *Rgs9* – had causal effects on its expression in the mouse

striatum. These data provide important clues as to the impact of ethanol on striatal biology and provide a key resource for future investigation.

B. Introduction

Alcohol Use Disorder (AUD) is characterized by compulsive intake of alcohol, often following a chronic, relapsing pattern over many years. AUD affects >5% of the global population and is associated with enormous medical and economic consequences, including ~140,000 annual deaths from alcohol-related causes in the United States alone.[18] Only three medications are approved for AUD treatment in the United States, and they each provide limited efficacy.[74] The development of effective therapies is hindered by an incomplete understanding of alcohol's effects in the brain.

The dorsal striatum is a key structure dysregulated in humans with AUD, as well as in animal models of chronic alcohol intake.[20] The dorsal striatum is the input nucleus of the basal ganglia, receiving excitatory glutamatergic inputs from the thalamus and cortex, as well as modulatory dopaminergic inputs from the substantia nigra pars compacta.[2] Outputs from the striatum are funneled through two distinct pathways -- the "direct" striatonigral pathway and "indirect" striatopallidal pathway -- which have distinct, often opposing effects on the activity of downstream circuit elements in the pallidum, thalamus, and other regions.[4–6] GABAergic spiny projection neurons (SPNs) comprise ~95% of striatal neurons. Molecularly distinct SPN subtypes marked by expression of D_1 vs. D_2 dopamine receptors form the direct and indirect pathways, respectively. SPNs are modulated by GABAergic and cholinergic interneurons and supported by numerous subtypes of glia and other non-neuronal cells.

Alcohol actions on the dorsal striatum are thought to foster the expression of actions related to alcohol seeking and its compulsive consumption.[75] Ethanol is a highly promiscuous ligand, and complex, cell-type specific physiological sequelae in dorsal striatum arise secondary to alcohol exposure.[45] Major neuronal physiological effects of ethanol influence glutamatergic synapses, GABAergic synapses, and morphological and intrinsic excitability.[27–31,37–39,76] Several modulatory transmitter systems in the dorsal striatum are also affected by alcohol, including brain-derived neurotrophic factor (BDNF) signaling, acetylcholine, endocannabinoids, opioids, and dopamine.[34,35,77–79] Given this complexity, there is a need for cellular-resolution studies to understand the nature of these diverse effects and the cellular sources of the expression changes driving them.

Single-nuclei RNA sequencing (snRNA-seq) has emerged as a powerful strategy to describe the cell type-specific molecular adaptations associated with exposure to addictive substances.[40,41] To date, only a few snRNA-seq studies have described changes in AUD or AUD-related animal models. snRNA-seq studies of the prefrontal cortex revealed cell type-specific transcriptional changes both in humans with AUD and in an animal model of chronic intermittent ethanol exposure.[42–45] snRNA-seq of the ventral striatum in a cohort of AUD cases and controls detected a small number of differentially expressed genes but was likely underpowered.[80] However, to our knowledge, there have been no published reports describing snRNA-seq of the striatum from an animal model of chronic ethanol exposure. Here, using snRNA-seq, we describe cell type-specific transcriptional changes in the dorsal striatum of mice exposed to chronic intermittent ethanol (CIE).

C. Methods

Animals: Male and female C57BL/6J mice were co-housed with littermates (2–5 per cage) under a 12-h light/dark cycle (lights on at 0700 hours) with ad libitum access to food and water. All experiments were performed in accordance with NIH guidelines and were approved by the Institutional Animal Care and Use Committee of the University of Maryland Baltimore.

Chronic Intermittent Ethanol (CIE): Mice were placed in Plexiglass inhalation chambers (60x36x60 cm) and exposed to ethanol vapor or air 16 hours/day, 4 days a week for a total of 5 weeks. Ethanol was volatilized by passing air through a tube submerged in 95% ethanol. After 4 days in the inhalation chambers, mice underwent a 72-hour forced abstinence period from ethanol. Control vapor chambers delivered only air without ethanol vapor. Vapor chamber ethanol concentrations were monitored daily, and air flow was adjusted to produce ethanol concentrations within 1.8-2.0 % ethanol content measured by a digital alcohol breath tester (FFtopu). These conditions produce stable blood ethanol concentrations in C57BL/6J mice ranging from 150-200mg/dl.[81] The alcohol dehydrogenase inhibitor pyrazole (1 mmol/kg, i.p.) was injected daily in weeks 4-5 to stabilize blood ethanol concentrations.

Tissue Collection: Following 5 weeks of ethanol exposure, mice were sacrificed by rapid decapitation and brains were immediately removed for tissue collection. The dorsal striatum (AP: +1.3 - 0.3 from bregma) was dissected from a 1mm coronal section cut from a mouse brain mold.[75] Left and right hemispheres were pooled, and flash frozen in crushed dry ice. The tissue was stored at -80°C until further processing. Our primary,

discovery dataset included sixteen C57BL/B6 mice equally divided between male and female. Each of our replication datasets included 8 mice equally divided between male and female.

Isolation of cellular nuclei and single-nuclei RNA sequencing (snRNA-seq): Distinct nuclei isolation protocols were used in the discovery dataset and in each of the two replication datasets. For the discovery dataset, cellular nuclei were isolated from frozen dorsal striatal tissue following a 10x Genomics Demonstrated Protocol (CG000124.RevE) with modifications. One hemisphere, dorsal striatum 1 mm punch, was used for 150ul lysis buffer for nuclei extraction. To remove cellular debris and large clumps, an Iodixanol density gradient was used. An 8.5% iodixanol (OptiPrep™ Density Gradient, Millipore) buffer serves as a cushion to remove membranes at 1000xg/10 min at 4C. Clean nucleus was collected in the pellet. Propidium iodide was used to determine the nuclei concentration using a bench cytometer MoxiGoII (Orflo) and nuclei aggregation and clumping were evaluated under 60X magnification in a fluorescent microscope and brightfield. Nuclei from one male mouse and one female mouse of the same ethanol treatment group were pooled. Approximately 20,000 nuclei per pooled sample were loaded into a Chromium X microfluidics controller (10x Genomics, Pleasanton, CA). 10x Genomics NextGEM 3' GEX sequencing libraries were prepared from each sample following manufacturer's instructions and sequenced at depth of 50M/sample on HiSeq4000 Sequencer.

For both replication datasets, nuclei were isolated from frozen brain tissue following a published protocol with our slight modifications.[82,83] Briefly, frozen brain tissue was disaggregated by pipetting up and down in chilled extraction buffer consisting of Poly(1-

vinylpyrrolidone-co-vinyl acetate) (Sigma #190845), 0.1% TritonX-100, and 1% bovine serum albumen (BSA) in dissociation buffer (DB; 82 mM Na2SO4, 30mM K2SO4, 10mM Glucose, 2.5mM MgCl2,10mM Hepes pH7.4, and RNase inhibitor [Protector, Roche]). Pellets containing nuclei were resuspended in DB and filtered with 70 um and 40 um strainers. To separate nuclei from debris, the nuclei suspension was mixed in a 25% (final) iodixanol layer over a 27% iodixanol cushion, followed by centrifugation (13000g x 20min, 4° C), then nuclei were washed twice in DB. In the second replication dataset, nuclei were labeled with sample-specific oligonucleotide tag using CellPlex reagents, following a validated protocol (CG000391). Finally, nuclei were counted using a MoxiGoII (Orflo) cytometer, and the concentration was adjusted to 365 nuclei/ul in phosphate buffered saline with 2% BSA. 17,000 nuclei were loaded in each well of a Chromium Controller (10x Genomics). Nuclei from four male and four female mice were pooled in each sample. Sequencing libraries were prepared using NextGEM 3' Gene Expression reagents (10x Genomics), following manufacturer's instructions and sequenced on HiSeq4000 (Replication Dataset 1) and NovaSeq6000 (Replication Dataset 2) sequencers.

snRNA-seq data analysis: Genome alignment (mm10), cell calling, and read counting were performed with cellranger count (v7.1.0), Doublets were detected and removed via scDblFinder.[84] Cells then underwent standard quality control and gene expression data processing with Seurat.[85] Cells with a minimum of 500 reads, no more than 5000 reads and a mitochondrial percentage less than 20 were selected for initial inclusion. Integration was accomplished using Seurat's SCTransform() pipeline, using 3000 features as integration anchors. Cell clusters were obtained via Louvain clustering

(resolution = 0.5) of a shared nearest neighbors graph derived from the first 30 principal components of the integrated data. We applied Uniform Manifold Approximation and Projection to visualize the clusters on two-dimensional plots. We assigned clusters to major cell types based on established markers. We repeated this process, dropping three clusters with mixed markers, as these most likely represent doublets.[86] One of the dropped clusters included low level expression of both iSPN and dSPN markers without evidence of eSPN markers. The other two clusters dropped exhibited mixed oligodendrocyte/astrocyte markers. Neuronal and non-neuronal subtypes were then separated, and the same dimension reduction and clustering procedures were completed within each grouping to refine subtype clustering and identification. We recombined these results and completed two additional iterations of clustering, dropping two additional clusters with iSPN/dSPN mixed markers and no evidence of eSPN markers, as these most likely represent doublets.[86] As noted above, library preparation and sequencing were performed using pooled cells from male and female mice. We demultiplexed the male vs. female cells within each pooled sample based on the universally expressed female-specific marker gene *Xist.* First, we performed zero-preserving imputation of read counts with ALRA[87] to reduce dropouts. Then, cells with normalized *Xist* expression values greater than the median were assigned as female, and cells with expression values below the median were assigned as male. We validated that Y chromosome genes were expressed near-exclusively in cells assigned as male. We note that as with all multiplexing strategies a small proportion of cells are ambiguous, and in this case cells with low read counts tend to be called as male by our algorithm. This is accounted for as a batch effect in the downstream analyses of differential gene expression

and network reconstruction (see below), and we believe it has minimal impact on our estimates for the effects of ethanol exposure. However, estimates for the main effects of sex are not presented, as these may be unreliable due to the bias toward lower read counts in cells assigned as male.

Effects of ethanol exposure on differential gene expression in each cell type were calculated using negative-binomial generalized linear models implemented with edgeR[88], based on the pseudobulk read counts pooled from all the cells of each cell type in each mouse. Pseudobulk analysis avoids anticonservative p-values that have been encountered in models that treat individual cells as the unit of replication.[89] In our discovery dataset, we used ComBat-seq[90] (implemented in the sva R package) to adjust for batch effects across eight sample processing batches, corresponding to a male batch and female batch for each day on which samples were processed. Samples for each of the two replication datasets were processed separately, so no batch correction was performed. We filtered out genes with very low expression in the batch-corrected, pseudobulk read counts (minimum total reads = 15, including a minimum of 3 counts in one sample). We then fit the counts to a quasi-likelihood generalized linear model and estimated the effects of ethanol using the glmQLFit() and glmQLFTest() functions from the edgeR R package. Differential gene expression analysis was performed separately in each dataset and cell type. We then performed meta-analyses using the sum of weighted z-scores, where the weights were proportional to the number of cells of each cell type within each dataset. A "replication meta-analysis" was performed to combine the two replication datasets to obtain the replication results shown in Figure 2. A meta-analysis combining all of the discovery and replication datasets was used to produce the p-values used in downstream analyses. If a

cell type was represented by fewer than 100 cells in a dataset, that dataset was excluded from the meta-analysis. A significance threshold was set globally across all cell types at a False Discovery Rate (FDR) < 5%. P-values from the meta-analysis were used in downstream analysis. For analyses that required fold change estimates, we used the fold changes from the discovery dataset. For comparisons of differentially expressed genes across cell types, we further filtered out genes that had 10-fold higher expression in another cell type, based on pseudobulk counts per million. This filter was intended to reduce false-positive correlations between cell types due to ambient RNA.

Gene set enrichment analysis: Gene sets from Gene Ontology, SynGO, and KEGG were downloaded from the Enrichr database (HTTps://maayanlab.cloud/Enrichr/#libraries) on December 6, 2023. For gene set enrichment analyses of cell type differentially expressed genes, we applied the geneSetTest() function from the limma R package to test enrichments among up- and down-regulated genes (separately) from each cell type.[91] For gene set enrichment analysis of gene co-expression modules we tested for enrichment using Fisher's exact tests. For visualization purposes, we calculated Cohen's kappa to compare gene sets and plotted only those terms for which not term with $k > 0.5$ had a stronger p-value.

Gene co-expression networks: Gene co-expression modules in spiny projection neurons were identified via an imputation and clustering procedure, with slight modifications from our published work.[92] We started from the read counts in 8,535 dSPNs, iSPNs, and eSPNs from our snRNA-seq of four mice processed on the same day (discovery dataset in Table S2.1; one per sex per group). Selecting cells from a single processing batch was intended to reduce technical variation among the samples. We removed genes with read

counts in fewer than 3% of these cells. Read counts were imputed with ALRA to improve correlation structure in the data, followed by normalization as counts per million, log-transformation, zero-centering, and scaling to unit variance. Next, we performed k-means clustering using the kmeans() function in R with k=50, Lloyd's algorithm, 10 starts, and up to 10,000 iterations. Finally, the clustering results were refined by merging clusters whose centroids were strongly correlated (Pearson's $r > 0.7$) and by removing genes that were weakly correlated with the centroid of the module to which they had been assigned ($r < 0.3$). We tested for enrichment of modules among differentially expressed genes using Fisher's exact tests, using a lenient differential expression threshold ($P < 0.01$) to improve statistical power. Hub genes were identified by ranking each module's genes by their correlation with the module centroid. For visualization purposes, we scored the expression of modules across our entire snRNA-seq dataset using the addModuleScore() function in Seurat.

Replication analyses with mRNA-seq of human striatum. Differential gene expression statistics from mRNA-seq of the caudate nucleus in alcohol use disorder cases vs. controls were obtained from Table S2 in Zillich et. al. (2022).[46] We used the limma geneSetTest() function to test the hypothesis that differentially expressed genes from our snRNA-seq of CIE-exposed mice (FDR < 0.05 in any cell type) were enriched for up- or down-regulated gene expression in AUD cases vs. controls. In addition, we used the geneSetTest() function to test for up- or down-regulation of the genes in each gene co-expression module.

Analysis of mRNA-seq from the striatum of mice heterozygous for Module M43 hub genes. Wang et al. (2022) performed mRNA-seq of striatal tissue from six-month-old

heterozygous knockout mice and wildtype littermate controls for 52 genes (n=3 male and n=3 female mice per genotype).[93] Details of their study design are contained in the original paper. The genes investigated by Wang et al. were selected based on their expression patterns in the striatum of Huntington's disease knock-in mice. Seven of the genes overlapped Module M43 from our gene co-expression analysis, enabling us to test the hypothesis that each genetic perturbation causally regulates the expression of genes in Module 43. We downloaded the mRNA-seq read counts and sample metadata (GSE149900). We computed differential gene expression in each heterozygous genotype compared to wildtype controls using voom/limma, treating sex as a covariate.[94] We used Fisher's exact tests to evaluate whether the up- and down-regulated genes in each knockout line (FDR < 0.05) were enriched among the genes in M43.

Data and code availability. Sequencing data are being submitted to the Gene Expression Omnibus (accession # in progress). Code used in the data analysis is available at www.github.com/seth-ament/cie-snrnaseq. All other data are presented in the main text and supplementary figures and tables.

D. Results

A single-cell genomic atlas for the effects of chronic ethanol exposure in the dorsal striatum

Chronic Intermittent Ethanol (CIE) is a widely used paradigm to model the effects of moderate to heavy alcohol consumption.[81,95,96] Previous studies have shown that CIE and related paradigms lead to cell type-specific physiological changes in striatal neurons, but the molecular mechanisms remain poorly understood. To gain insight, we performed 10x

Genomics single-nuclei RNA sequencing (snRNA-seq) in the dorsal striatum of four-month-old C57BL/6J mice that had undergone five weeks of CIE, compared to age- and sex-matched controls (Fig. 2.1A,B). We used a two-stage meta-analysis to discover and replicate effects of CIE. In our discovery dataset, we sequenced nuclei from n=8 CIE-exposed mice and 8 controls (n=4 male and female mice per group), yielding 70,934 high-quality cells (31,225 CIE, 39,709 controls). In our replication dataset, we performed snRNA-seq of pooled samples from 8 additional CIE-exposed mice and 8 controls, yielding 15,781 high-quality cells. The lower number of cells in the replication dataset is expected due to the pooling strategy. Data quality metrics are shown in Table S2.1.

Cells in each snRNA-seq dataset were clustered and assigned to 12 cell types based on established cell type markers (Fig. 2.1C,D; Fig. S2.1; Tables S2.2-S2.3). Neuronal subtypes included direct pathway spiny projection neurons (dSPNs; *Drd1*+), indirect pathway spiny projection neurons (iSPNs; *Drd2*+), atypical spiny projection neurons (termed "eccentric", eSPN; *Otof*+), cholinergic interneurons (IN-Chat; *Chat*+), parvalbumin interneurons (IN-PV; *Kit*+), and somatostatin interneurons (IN-Sst; *Sst*+). Non-neuronal cell types included astrocytes (*Slc1a3*+, *Rorb*+), oligodendrocytes (*Mog*+, *Aspa*+), oligodendrocyte precursor cells (*Pgdfra*+, *Coll11a1*+), mural cells (*Vtn*+, *Pgdfrb*+), endothelial cells (*Flt1*+, *Slco1a4*+), ependymal cells (*Rsph1*+), and microglia (*Cx3Cr1*+, *C1qc*+). We note that eSPNs represent a heterogeneous population represented by two distinct clusters on the UMAP (Fig. 2.1C).

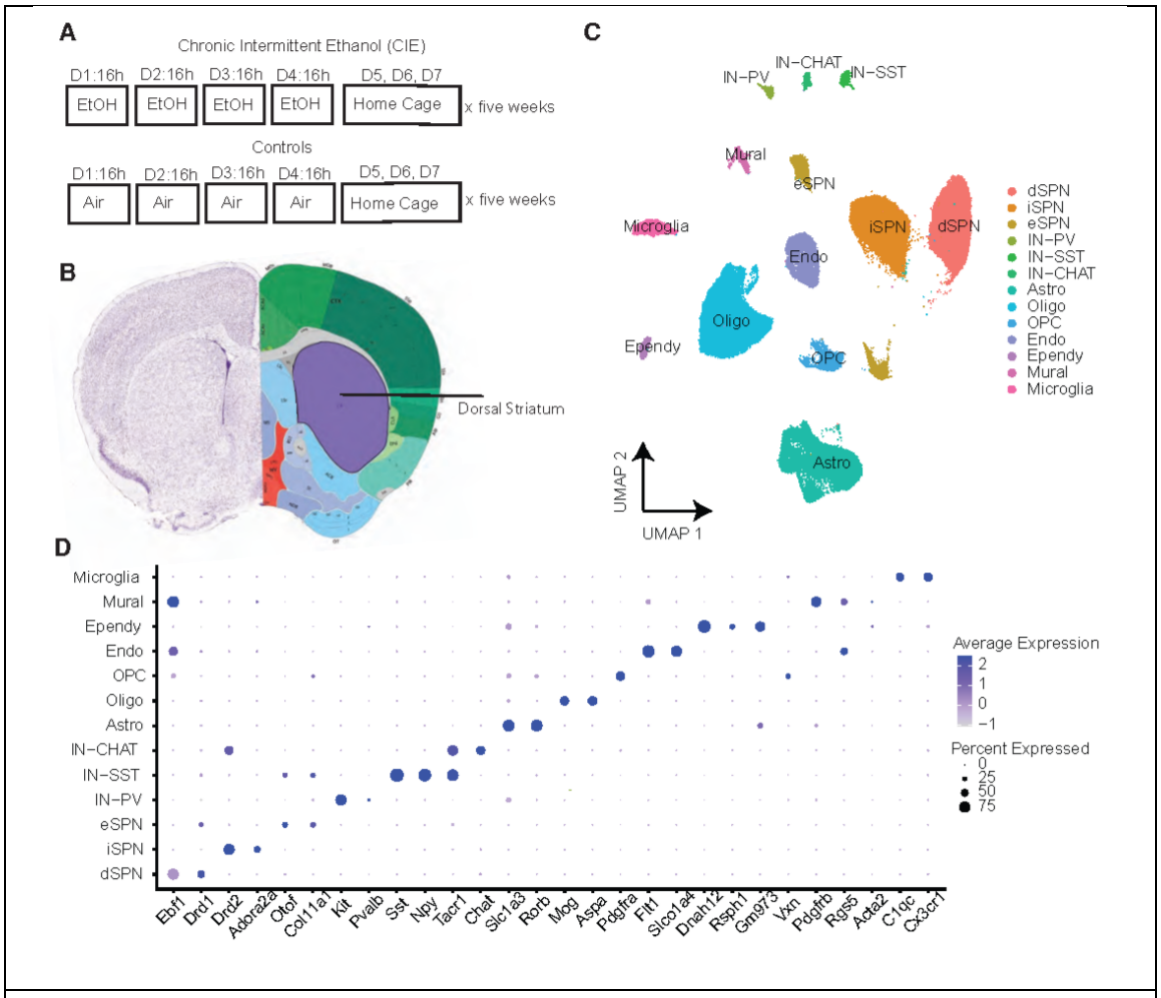

Figure 2.1. Single-nuclei RNA sequencing of the mouse dorsal striatum in the context of chronic intermittent ethanol exposure. A. The chronic intermittent ethanol (CIE) paradigm. B. Location of the dorsal striatum on a coronal section of the mouse brain (reproduced from the Allen Reference Atlas). C. Uniform manifold approximation and projection (UMAP) plot displaying snRNA-seq cell clusters from the discovery dataset. D. Dot plot for the expression of cell type marker genes in the discovery dataset. D1-D7, days 1-7; SPN, spiny projection neurons; IN, interneurons; Astro, astrocytes; Oligo, oligodendrocytes; OPC, oligodendrocyte precursor cells; Endo, endothelial cells; Ependy, ependymal cells.

We characterized differentially expressed genes (DEGs) in CIE-exposed vs. control animals using a conservative pseudobulk approach and compared our discovery and replication datasets to assess reproducibility. In our discovery dataset, we found 497 cell type specific DEGs at a False Discovery Rate (FDR) < 0.05. DEGs were identified in all

cell types, yet the vast majority were detected in SPNs, with 176, 92, and 135 DEGs in dSPNs, iSPNs, and eSPNs, respectively, compared to fewer than 30 DEGs in all other cell types (Fig. 2.2A; Table S2.4).

In our replication dataset, we found 460 cell type specific DEGs at FDR < 0.05, and again DEGs were detected primarily in SPNs (Fig. 2.2A, middle; Tables S2.5-S2.7). 37 DEGs were reproducible at FDR < 0.05 in both the discovery and replication datasets (more than expected by chance: Fisher's exact test, odds ratio = 33.9, P = 6.2e-50). In addition, 141 of the 497 DEGs from the discovery dataset replicated at a nominal p-value < 0.05. Notably, most of the highly reproducible DEGs were down-regulated in both dSPNs and iSPNs, with somewhat stronger p-values but similar fold changes in dSPNs (Fig. 2.2B). Most of these genes were differentially expressed specifically in SPNs and not in other striatal cell types (Fig. 2.2C).

We applied a threshold-free approach, rank-rank hypergeometric overlap (RRHO)[97], to evaluate the reproducibility of differential expression patterns in specific cell types. This analysis revealed significant reproducibility of differential expression ranks (FDR < 0.05) in dSPNs, iSPNs, eSPNs, IN-PV, astrocytes, and OPCs, again with the strongest effects in SPNs (Fig. 2.2D). We note that three rare cell types – endothelial cells, mural cells, and cholinergic interneurons – were detected too infrequently in the replication dataset (fewer than 100 cells each) to be included in these analyses of reproducibility, though each displayed intriguing effects in the discovery dataset.

We performed a meta-analysis across the discovery and replication datasets to obtain a final list of differentially expressed genes. In the meta-analysis, we detected 462 DEGs at FDR < 0.05, including 248, 82, and 94 DEGs in dSPNs, iSPNs, and eSPNs, respectively,

and ten or fewer DEGs in each of the other cell types (Fig. 2.2A, right; Table S2.8). We used p-values from the meta-analysis in downstream analyses.

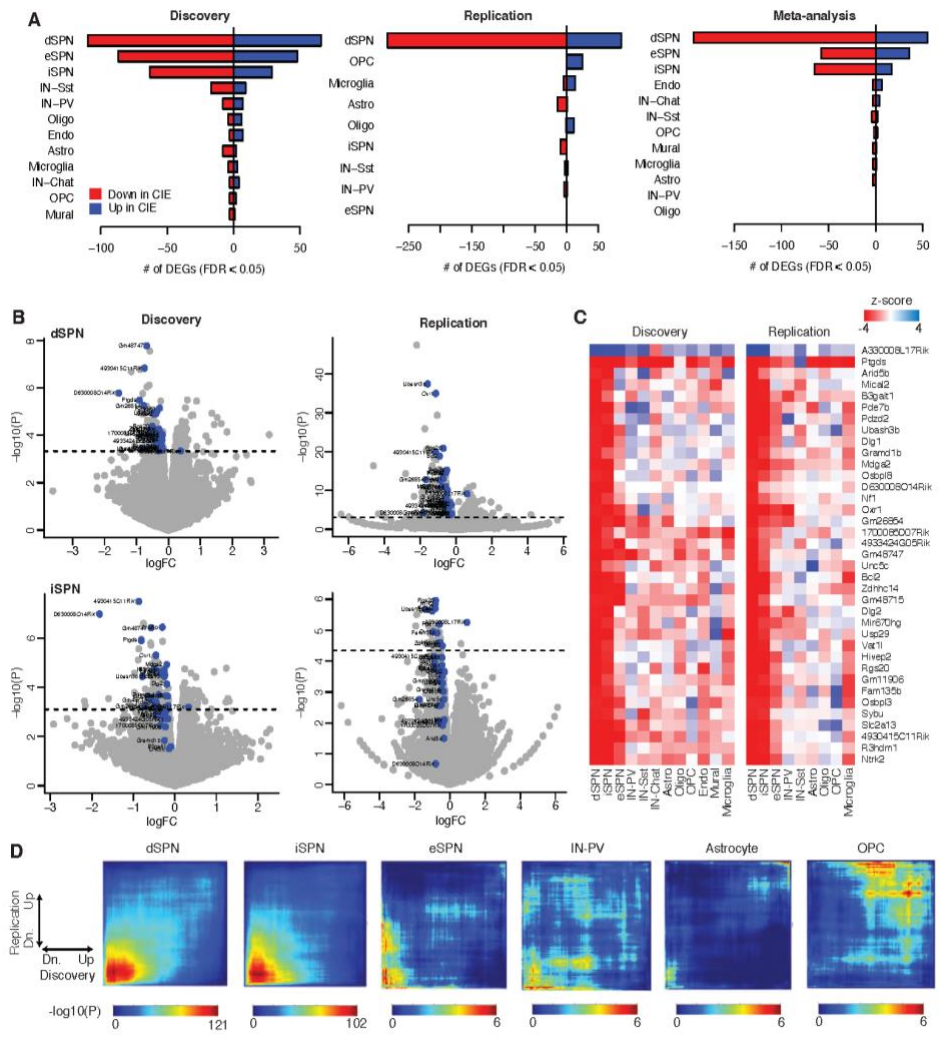

Figure 2.2. Discovery and replication of differentially expressed genes in dorsal striatum cell types from chronic intermittent ethanol (CIE)-exposed vs. control mice. A. Counts of cell type-specific differentially expressed genes (DEGs; False Discovery Rate [FDR] < 0.05) in the discovery samples, replication sample, and meta-analysis. B. Volcano plots showing the log2(fold change) and -log10(p-value) for differential gene expression in the discovery and replication samples. Dashed line corresponds to FDR < 0.05. 37 highly-reproducible DEGs with FDR < 0.05 in both samples (primarily in dSPNs) are labeled and highlighted in blue. C. Effect sizes for the 37 highly-reproducible DEGs across cell types in the discovery and replication samples. D. Rank-rank hypergeometric overlap plots visualizing the reproducibility of differential expression ranks within six cell types for which the reproducibility was greater than expected by chance (FDR < 0.05). Heatmap color indicates the hypergeometric -$\log_{10}$(p-value) for the overlap between the differential expression gene ranks at multiple thresholds within the discovery and replication datasets. Significant p-values in the lower-left quadrant of each plot indicate reproducible down-regulation in CIE-exposed vs. control mice, while significant p-values in the upper-right quadrant indicate reproducible up-regulation.

Shared vs. cell type-specific effects of ethanol exposure across striatal cell types

Next, we performed gene set enrichment analyses to characterize the functional categories perturbed in each cell type, and we compared these effects across cell types. We used a threshold-free algorithm, limma's geneSetTest[91], which enabled us to find significant gene sets even for cell types in which no individual DEGs were detected. These analyses revealed both cell type-specific gene sets enriched for up- or down-regulated genes, as well as gene sets that were dysregulated in multiple cell types (Fig. 2.3; Table S2.9).

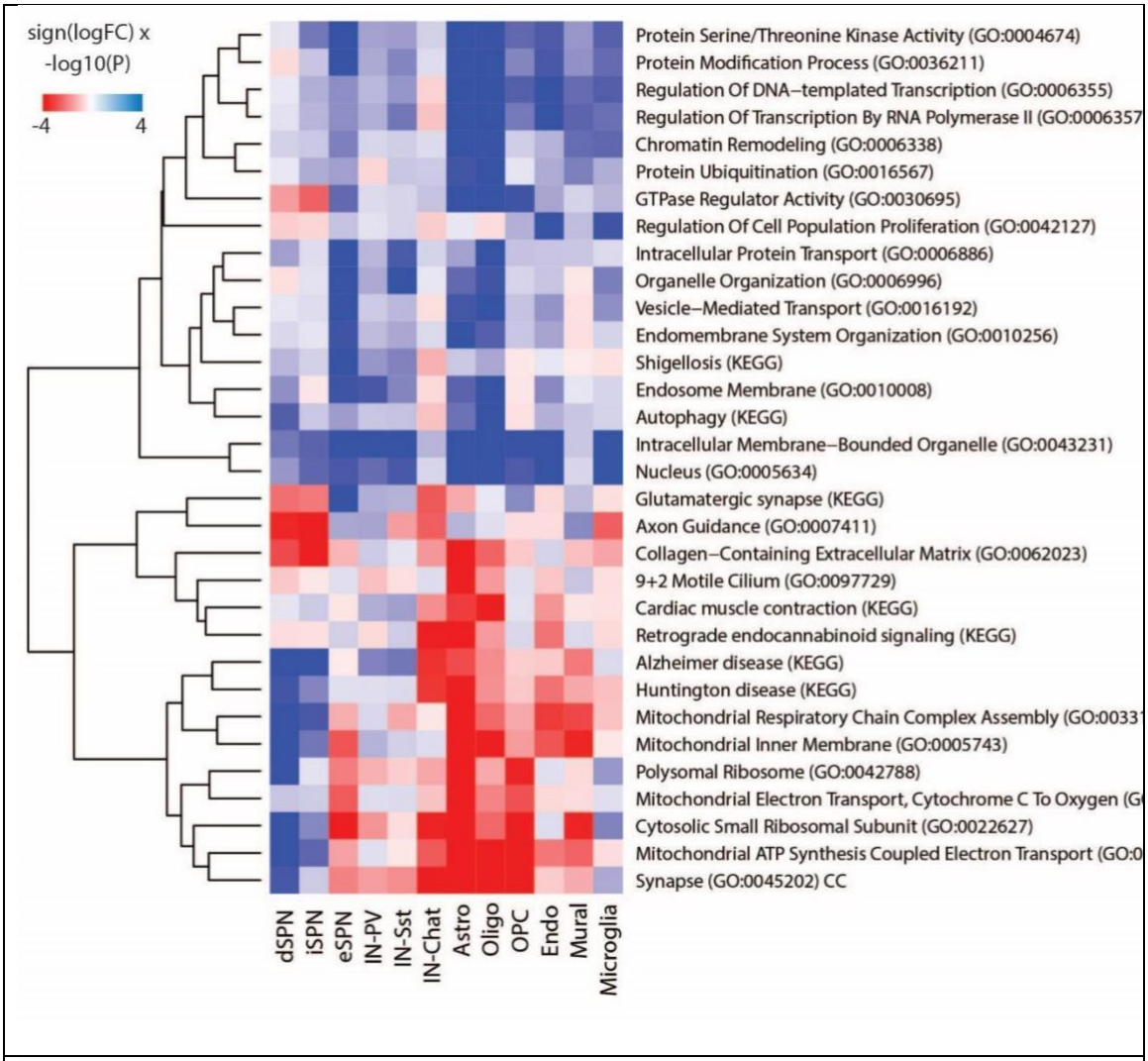

Figure 2.3. Gene sets enriched for differential gene expression in CIE vs. control mice. A total of 217 Gene Ontology and KEGG gene sets were enriched among the differentially expressed genes, significant in at least one cell type at FDR < 0.05. The top 30 gene sets are shown after dropping redundant sets that had substantial overlap with a more-significant set (Cohen's kappa > 0.5). $\log_{10}$(p-values) of 4 or larger are indicated by saturated heatmap colors.

Amongst the more cell type-specific effects, we found that synapse-related gene sets, including components of glutamatergic synapses and genes involved in axon guidance were down-regulated primarily in spiny projection neurons: Glutamatergic Synapse (KEGG) in dSPNs, P = 6.3e-3; in iSPNs, P = 6.8e-3; Axon guidance (GO:0007411), in dSPNs, P = 2.5e-4, in iSPNs, P = 9.2e-9. Down-regulated components of glutamatergic

synapses in dSPNs (FDR < 0.05) included the synaptic scaffolding protein *Homer1*, the voltage-gated calcium channel subunit *Cacna1a*, and the glutamate receptor subunits *Grm5, Grik2,* and *Gria4.* In the adult brain, many axon guidance genes help maintain synapses. Down-regulated genes annotated to this pathway included *Reln, Unc5c,* and *Plxna1*, amongst others. These results suggest a specific vulnerability of spiny projection neuron synapses to chronic intermittent ethanol.

We also found cell type-specific effects of ethanol exposure in endothelial cells, including enrichment of endothelial DEGs for genes involved in the regulation of cell population proliferation (GO:0042127, P = 1.3e-6). Differentially expressed genes in this category (FDR < 0.1) included the Notch effector *Hes1* (down-regulated, unadjusted P = 2.9e-5), as well as *Tgfb2,* which encodes transforming growth factor-beta 2 (up-regulated, P = 6.0e-5). Endothelial cells are the major cell type of blood vessels in the brain, so we speculate that these changes may relate to the effects of ethanol exposure on angiogenesis.[98–100]

Several categories of genes were dysregulated across multiple cell types. For instance, at FDR < 0.1, components of ribosomes (KEGG, "Ribosome") were enriched for differential gene expression in eight cell types. Genes involved in the regulation of transcription by RNA Polymerase II (GO:0006357) were up-regulated in astrocytes, oligodendrocytes, and endothelial cells. Genes involved in mitochondrial ATP synthesis-coupled electron transport were down-regulated in astrocytes, OPCs, and oligodendrocytes but up-regulated in dSPNs. These results suggest complex effects of ethanol on the regulation of transcriptional and energy metabolism.

We studied the fold changes of individual DEGs across cell types to gain further insight into these shared vs. cell type-specific effects. First, we calculated the correlations of fold changes across all DEGs. This analysis revealed strongly correlated effects of alcohol in dSPNs and iSPNs (Pearson's r = 0.86, P = 7.3e-89; Fig. 2.4A), and 53 genes were differentially expressed at FDR < 0.05 in both subtypes (Fig. 2.4B). A biplot revealed that nearly all DEGs have similar effects sizes in both of these SPN subtypes (Fig. 2.4C). Fold changes in eSPNs were somewhat more modestly correlated with fold changes in dSPNs (r=0.56) and iSPNs (r=0.54), and there were only 7 DEGs in common amongst all three SPN subtypes. Biplots confirmed a mix of shared and subtype-specific effects when comparing eSPNs to the canonical SPN subtypes (Fig. 2.4D,E). We also found more modest, positive correlations in fold changes in other cell types, reflecting the shared functional categories described above. Across all pairs of cell types, the median correlation coefficient among DEG fold changes was r=0.29 (Fig. 2.4A). 23 protein-coding genes displayed log2 fold changes greater than 0.25 in eight or more cell types (Table S2.8). These included *Ptger4*, encoding a prostaglandin receptor, *Egr1*, encoding an activity-dependent transcription factor, and *Ctnna3*, encoding alpha-catenin 3, each of which were down-regulated in most cell types (Fig. 2.4F). Overall, these results suggest that the transcriptional effects of alcohol in canonical SPN subtypes are nearly indistinguishable, and certain effects manifest in similar ways across nearly all striatal cell types.

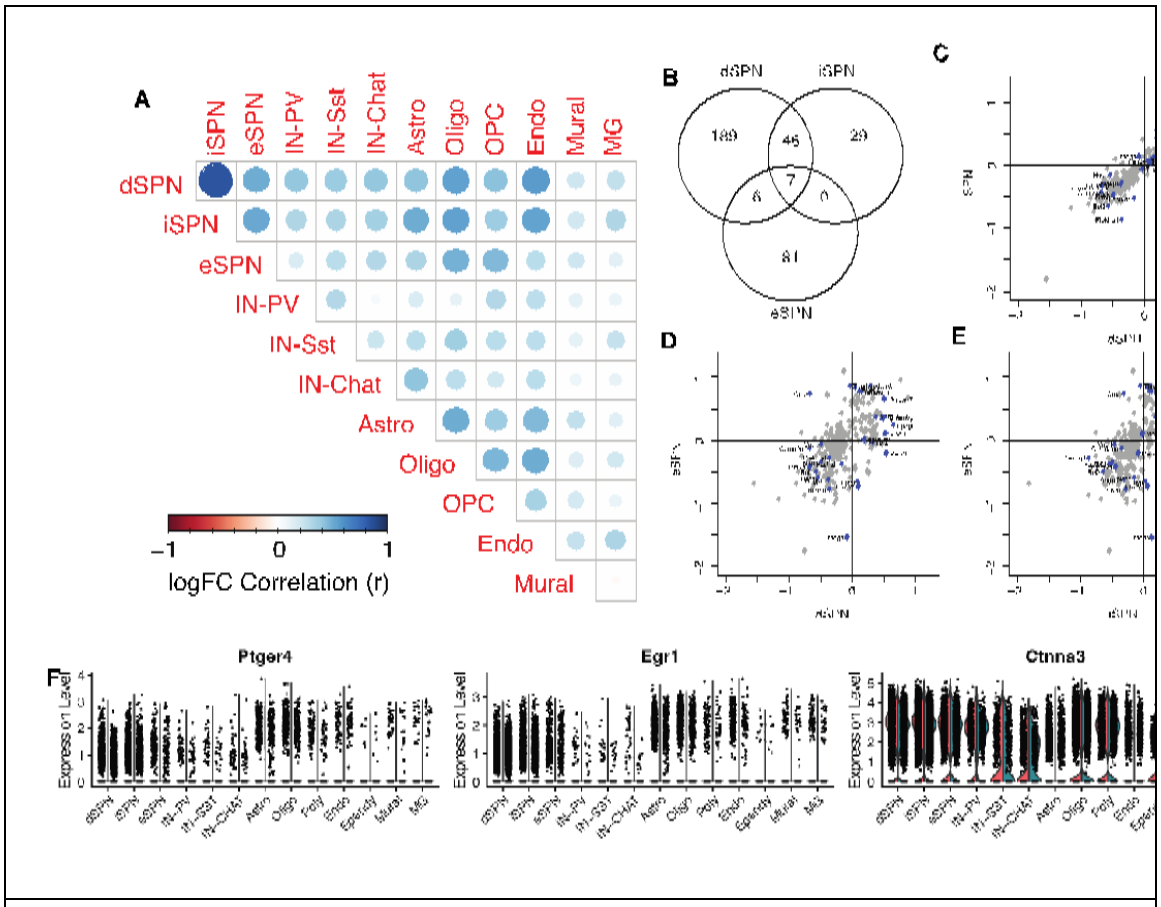

Figure 2.4. Correlated effects of alcohol across striatal cell types. A. Heatmap indicating the strengths of correlations between cell types based on the log2 fold changes of differentially expressed genes in chronic intermittent ethanol-exposed mice vs. controls. B. Venn diagram indicating the counts of shared vs. unique DEGs in dSPNs, iSPNs, and eSPNs. C-E. Biplots comparing the log2 fold changes of DEGs in dSPNs vs. iSPNs (C), dSPNs vs. eSPNs (D), and iSPNs vs. eSPNs (E). The top five up- and down-regulated DEGs in each cell type are labeled and highlighted in blue. F. Selected genes with abs(log2 fold changes) > 0.25 in eight or more cell types. For each cell type, the violin and points on the left and right indicate expression in CIE-exposed vs. exposed animals, respectively.

Dysregulation of synaptic and neuroinflammatory gene networks in spiny projection neurons

We performed a gene co-expression network analysis to further characterize the effects of ethanol exposure. We analyzed gene-gene correlation structure specifically within SPNs since they had the largest transcriptional responses. k-means clustering of SPN gene

expression profiles revealed 45 modules of co-expressed genes (Fig. 2.4A; Table S2.10). We prioritized CIE-related modules by testing each module's over-representation among differentially expressed genes in CIE vs. control animals (Fig. 2.4B; Table S2.1). This analysis again focused on SPNs, but we also tested for over-representation among DEGs in other cell types to determine whether some effects of alcohol may be broader.

Three modules (M29, M43, and M26) were over-represented among genes down-regulated in SPNs (Bonferroni-adjusted p-value < 0.01) with little evidence of differential expression in other cell types. M29 displayed similarly strong associations with CIE in the three SPN subtypes (dSPNs, iSPNs, and eSPNs), whereas M43 was primarily associated with DEGs in canonical SPNs (dSPNs and iSPNs) and M26 was most strongly associated with DEGs in eSPNs. These modules were enriched for genes with neuron-specific functions (Table S2.11). M29 was enriched for genes in the transmembrane receptor protein tyrosine kinase signaling pathway (7 genes, OR = 5.5, un-adjusted P = 5.2e-4), including the BDNF receptor *Ntrk2* (also known as trkB). M43 was enriched for genes in the calcium signaling pathway (11 genes, OR = 11.1, P = 3.0e-8) and other genes localized to glutamatergic synapses (9 genes, OR = 12.4, P = 2.1e-7), including components of voltage-gated calcium channels (*Cacnb2*, Cacna2d3), glutamate receptors (*Grid2*, *Grm5*, *Gria3*), and the cAMP signaling cascade (e.g., *Pde10a*, *Pde7b*, *Adcy5*, *Rgs9*). M26 was enriched for a variety of genes localized to neuron projections (43 genes, OR=3.1, P = 2.9e-9), including axon guidance genes (18 genes, OR = 4.1, P = 3.1e-6; e.g., *Sema6a*). These results support that chronic alcohol exposure leads to SPN-specific down-regulation of numerous synaptic components and related genes.

Module M8 was enriched for down-regulated DEGs in all three SPN subtypes, as well as in nearly all other neuronal and non-neuronal cell types in the striatum. M8 was most strongly enriched for genes involved in cytokine-cytokine signaling interactions (10 genes, OR = 7.4, P = 5.5e-6), as well as other genes involved in the regulation of inflammatory responses (10 genes, OR = 3.9, P = 6.4e-4). These results suggest that chronic alcohol exposure leads to neuroinflammation-related transcriptional changes that impact most or all striatal cell types.

Two modules (M24 and M18) were enriched for up-regulated DEGs. M24 was up-regulated primarily in dSPNs, whereas M18 was up-regulated primarily in eSPNs. Both of these modules were comprised of genes with rather diverse functions. Functional enrichments for M24 included sequence-specific DNA binding (27 genes, OR = 2.3, P = 1.7e-4), but also actin cytoskeleton (19 genes, OR = 2.1, P = 0.004) and inorganic ion transmembrane transport (16 genes, OR = 2.2, P = 0.005). Functional enrichments for M18 included regulation of cell migration (13 genes, OR = 3.0, P = 0.001) and calcium ion binding (10 genes, OR = 3.2, P = 0.002). Thus, CIE was associated with diverse transcriptional effects that were relatively subtle and cell type-specific compared to down-regulated processes.

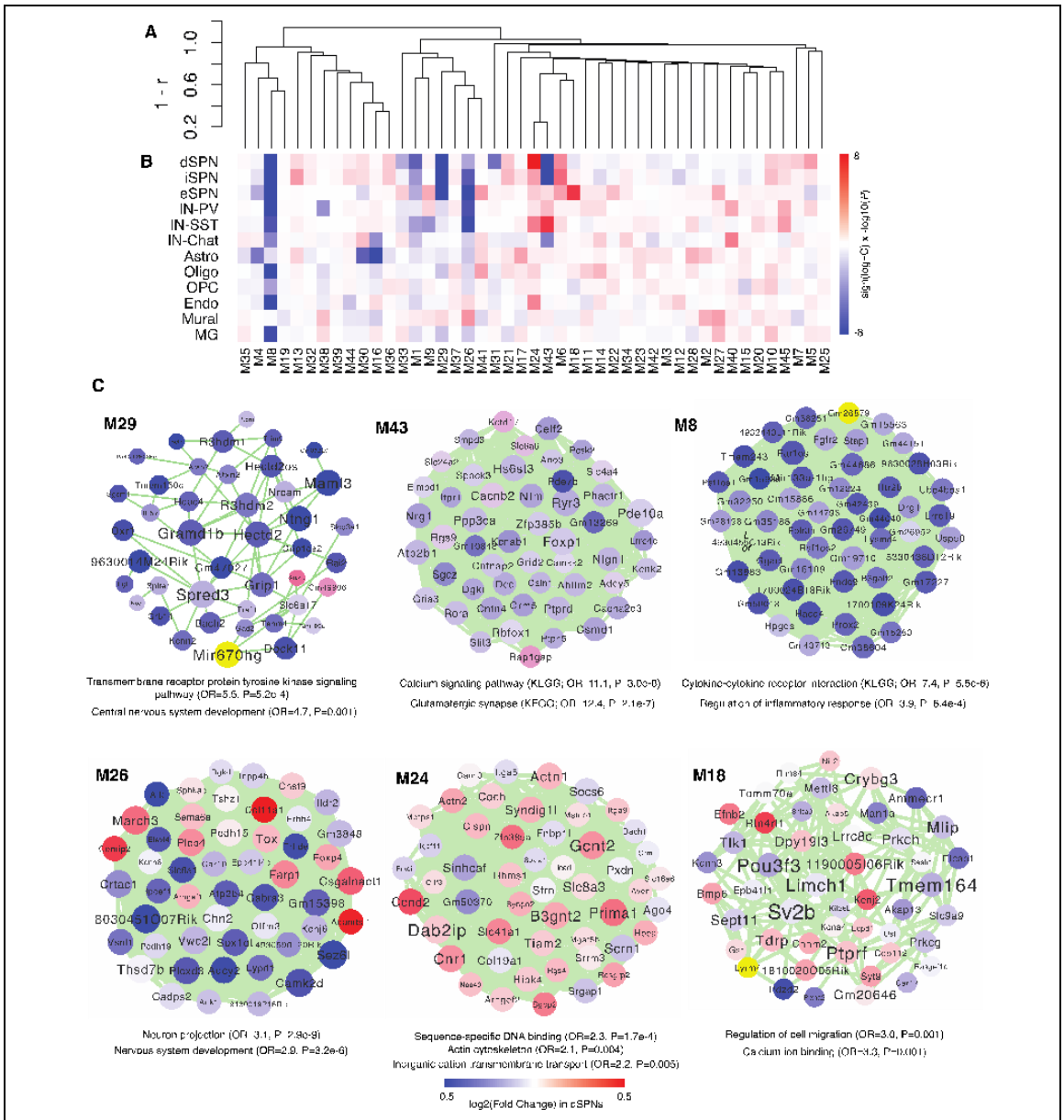

Figure 2.5. Gene co-expression networks dysregulated in spiny projection neurons after chronic intermittent ethanol. A. Hierarchical clustering of modules, based on the correlations of their centroids in spiny projection neurons. B. Enrichments of modules for differentially expressed genes in CIE vs. control mice. Blue and red shades correspond to enrichment for down- and up-regulated DEGs, respectively. C. The top 50 hub genes in each of six dysregulated modules. Node size corresponds to network centrality. Blue and red shades correspond to negative and positive fold changes in dSPNs from CIE vs. control animals, respectively. Gray lines connecting nodes indicate pairwise gene-gene correlations with Pearson's r > 0.5. We display 2-3 top Gene Ontology and KEGG gene sets over-represented in each module.

Reproducibility of molecular signatures in humans with alcohol use disorder and prioritization of drug targets

A central goal for transcriptomic profiling in animal models of disease is to identify therapeutic targets. We evaluated the translational potential for differentially expressed genes and gene networks in CIE-exposed mice via comparisons to published mRNA-seq from the caudate nucleus (a sub-region of the dorsal striatum) of humans who died with AUD vs. unaffected controls.[46] The authors reported very few differentially expressed genes at standard significance thresholds. Therefore, we performed a "sign test" to evaluate whether the differentially expressed genes that we detected in mice had fold changes in a concordant direction in humans. We found that genes down-regulated in our experiment (FDR < 0.05 in any cell type) were more likely to have negative fold-changes in humans with AUD than would be expected by chance (Fisher's exact test: odds ratio = 1.52, P = 0.004). 11 genes were down-regulated in our experiment at FDR < 0.05, as well as at a nominally significant p-value < 0.05 in AUD cases vs. controls (Table S2.13), including *Calhm2*, encoding an ion channel involved in calcium homeostasis, and *Apoe*, a lipoprotein known for its roles in neuroinflammation (Table S2.13). There was no equivalent replication for up-regulated genes.

We performed equivalent analyses to replicate differential expressed gene co-expression modules. One of the six CIE-associated modules, M43, had a strong pattern of differential expression in AUD cases vs. controls (Fisher's exact test on positive vs. negative fold changes in AUD: odds ratio = 5.3, p-value = 1.2e-12; Table S2.14). 84% of the 100 genes from M43 with human data had negative fold-changes in AUD cases vs. controls (Fig. 2.6A). M43 genes with the largest negative fold changes across the human

and mouse datasets included *Scgz*, encoding sarcoglycan Z, as well as the phosphodiesterase *Pde7b*. The fold changes observed in AUD cases were much smaller than those detected in ethanol-exposed mice, perhaps due to the high level of variability in human cohorts. These results provide evidence for concordant effects of alcohol exposure in CIE-exposed mice and humans with AUD.

Hub genes of gene co-expression modules are candidate drug targets because their perturbation frequently has causal effects on gene expression and on downstream physiological and behavioral traits. We therefore sought to prioritize drug targets within M43. First, we considered which genes in M43 are potentially targetable by small molecule or biotherapeutic drugs. 17 genes in M43 are repurposing candidates targeted by approved small molecules and biotherapeutic drugs and clinical-phase drug candidates (Fig. 2.6B, Tier 1).[101] An additional 19 genes in M43 are potentially druggable (Fig. 2.6B, Tiers 2 and 3). These candidates encode proteins in druggable gene families, including G protein (heterotrimeric guanine nucleotide–binding protein)–coupled receptors (GPCRs), nuclear hormone receptors, ion channels, kinases, and phosphodiesterases, as well as genes that encode secreted or extracellular proteins that can be targeted with monoclonal antibodies and related biotherapeutics. Thus, M43 includes a rich collection of potential drug targets.

Finally, we tested causal roles for M43 hub genes as regulators of M43 gene expression. For this purpose, we analyzed publicly available mRNA-seq of bulk striatal tissue from six-month-old mice heterozygous for each of seven M43 hub genes. These data were originally generated as part of a large study to evaluate drug targets for Huntington's disease, in which many of these same genes are dysregulated.[93] The tested genes included

four transcription factors (*Bcl11b*, *Foxp1*, *Rarb*, and *Zswim6*), as well as *Pde10a*, a phosphodiesterase, *Rgs9*, a negative regulator of G-protein signaling, and *Itpr1*, encoding the inositol 1,4,5-trisphosphate receptor, a calcium channel localized to the endoplasmic reticulum. Haploinsufficiency for *Bcl11b*, *Foxp1*, *Pde10a*, and *Rgs9* each resulted in gene expression changes that significantly overlapped M43 (Fig. 2.6C; Tables S2.14, S2.15). Haploinsufficiency for *Bcl11b*, *Foxp1*, and *Pde10a* primarily caused down-regulation of genes in M43, whereas haploinsufficiency for *Rgs9* caused upregulation of M43. These results suggest causal roles for these four genes in the regulation of M43 gene expression.

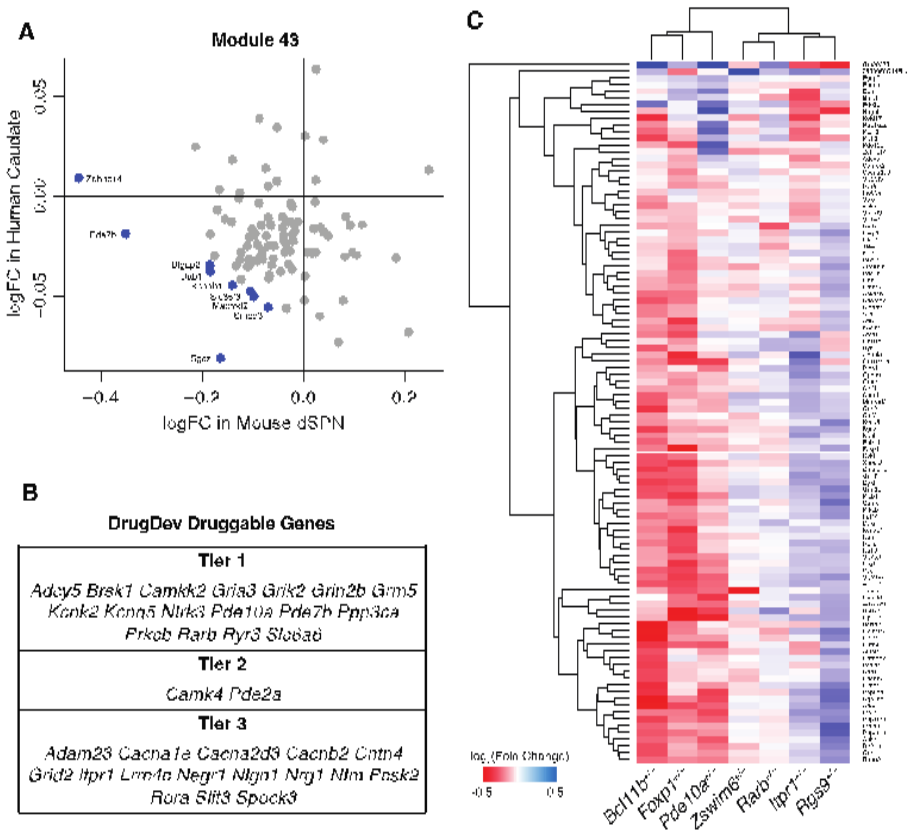

Figure 2.6. Translational potential for targeting Module M43 in alcohol use disorder. A. Log2 fold changes for genes in Module M43, comparing snRNA-seq of dSPNs from ethanol-exposed vs. control mice (x-axis) to mRNA-seq of bulk caudate nucleus tissue from human alcohol use disorder cases vs. controls.[46] The top genes by average effect size in mice and humans are highlighted and labeled. B. Categorization of druggable genes within M43 based on the DrugDev database.[101] Tier 1: targets of approved small molecules and biotherapeutic drugs and clinical-phase drug candidates. Tier 2: targets with known bioactive drug-like small-molecule binding partners or with >50% identity with approved drug targets. Tier 3: genes encoding secreted or extracellular proteins, proteins with more distant similarity to approved drug targets, and members of key druggable gene families not already included in tier 1 or 2 [G protein (heterotrimeric guanine nucleotide–binding protein)–coupled receptors (GPCRs), nuclear hormone receptors, ion channels, kinases, and phosphodiesterases]. C. Up- and down-regulation of M43 genes in the striatum of 6-month-old mice heterozygous for seven M43 hub genes.[93]

E. Discussion

The data presented here provide insight into the cell type-specific effects of chronic intermittent ethanol exposure on gene expression in the dorsal striatum, a key brain region implicated in AUD. The most robust finding was the downregulation in SPNs of genes involved in postsynaptic signaling cascades, a pattern that was reproducible in the post-mortem caudate nucleus of the dorsal striatum of humans with AUD. Neuroinflammation-related genes were also down-regulated in SPNs. Although we identified very few DEGs in non-neuronal cell types at stringent significance thresholds, the patterns of differential gene expression point to inflammation-related changes in many cell types, as well as potential angiogenic signatures in vascular cells. Finally, 37 druggable or potentially druggable targets were identified in module M43, which is enriched for synaptic signaling genes.

Multiple results suggested down-regulation of synaptic signaling pathways in SPNs. Notably, our network analysis revealed distinct down-regulated modules, M29 and M43, that were enriched for components of cAMP signaling and BDNF signaling, respectively. cAMP signaling components such as the M43 hub gene *Pde7b* act downstream of postsynaptic dopamine receptors in canonical SPNs. PDE7B is involved in the intricate balance of neuronal growth and pruning that shapes neuronal plasticity and has previously been implicated in neurodegenerative disease. Studies in neurodegenerative disease, especially Parkinson's disease, found that PDE7B inhibition attenuated neurodegenerative decline, possibly preventing the loss of dopaminergic neurons.[102–104] Phosphodiesterase inhibitors have been tested on a variety of brain disorders, including AUD.[105] In addition, dopamine signaling through the D1 receptor upregulates *Pde7b*,

suggesting a downregulation in D1 receptor signaling in chronic ethanol exposure, which is supported by literature highlighting dysregulation of dopaminergic signaling.[106–109]

The BDNF receptor *Ntrk2*/TrkB and other components of receptor tyrosine kinase signaling cascades were also downregulated in SPNs and were enriched in module M29. *NTRK2* is implicated in AUD.[110] *TrkB* acts as a high-affinity receptor for brain derived neurotrophic factor (BDNF), and also has affinity for neurotrophin-3 and neurotrophin-4. These peptides and signaling cascades are involved in diverse physiological processes including synaptic plasticity, differentiation, and neuronal growth.[110–112] In the striatum, BDNF originating from cortical and substantia nigra neurons binds TrkB to initiate several signaling cascades.[113,114] Unsurprisingly, since BDNF does not originate from striatal cells, the *Bdnf* gene did not exhibit a clear signal of differential expression in our analysis. This is despite the important role that dorsal striatal BDNF plays in gating alcohol consumption.[115]

Our analysis also shows down-regulation of a neuroinflammatory module, M8. M8 contains ten genes annotated to the cytokine-cytokine signaling pathway, most of which had negative fold-changes in multiple striatal cell types. Several of these genes encode receptors for the pro-inflammatory cytokines IL1, IL12, IL3, IL5, and TNF (*Il1r2*, *Il12rb2*, *Cx3cr1*, *Ccr9*, and *Tnfrsf9*, respectively). M8 also includes genes encoding erythropoietin (*Epo*) and leukemia inhibitory factor receptor (*Lifr*), which have anti-inflammatory functions[116–119]. Likewise, down-regulated genes in M8 annotated to the broader "inflammatory response" pathway included both pro-inflammatory (*Aim2*, *Lrrc12*, and *Ptgis*)[120–122] and anti-inflammatory genes (*Fbxl2, Ptger4 Otulin, Spata2, Gps2)*.[123–127] Thus, chronic ethanol exposure in this mouse model was associated with the

suppression of both pro- and anti-inflammatory genes, suggesting a complex change in inflammatory state. Down-regulation of these genes may be surprising, as studies of AUD have consistently found increases in circulating cytokines and markers of neuroinflammation.[128–131] The innate immune response to chronic alcohol, facilitated by TLR receptors, pro-inflammatory cytokines and complicated signaling between microglia and other cell types, has been identified as a key element of AUD with the potential for druggable targets.[132] Acute vs. chronic phases of inflammation often involve bidirectional changes in the expression of inflammatory signaling cascades, so one explanation may be that our mouse model captures a different stage of inflammation than that captured in many studies of AUD in humans. Alternatively, the downregulation of pro-inflammatory receptors in the brain may be a response to an increase in peripheral cytokines and neuroinflammation. There is a need for additional studies to further characterize these inflammatory signatures and their relationship with the changes in neural circuit function.

Despite lower statistical power for rare cell types, our data also suggest altered states of non-neuronal cell types. For instance, our data support angiogenesis-related gene expression changes in endothelial and mural cells. Top DEGs in endothelial cells included *Hes1*, *Tmem252* and *Tgfb2*. *Hes1* is a transcription factor that acts as an effector for the Notch signaling pathway, whose activation inhibits vascular cell differentiation and angiogenesis.[133,134] Down-regulation of Notch1 and Hes1 promote angiogenic cell sprouting and inhibit vascular repair following insult.[133,135,136] *Tmem252* is a stalk-cell marker involved in angiogenesis and neovascularization. *Tgfb2* encodes for TGF-B2, which is a dynamic actor that can either inhibit or support angiogenesis.[137,138] A fourth gene, *Ttr*, encoding transthyretin, was also identified as a down-regulated gene. *Ttr* is

primarily expressed in choroid plexus cells[139] [140,141], which were rare in our dataset and were not annotated as a distinct cell cluster. Nonetheless, the finding is intriguing, as *Ttr* is a potent inhibitor of angiogenesis[142143]. Thus, although there were few DEGs in endothelial cells, many can be interpreted as indicators of increased angiogenesis after CIE. An increase in angiogenesis in response to ethanol exposure may disrupt the blood brain barrier and play a role in the neuroinflammation seen in CIE, as has been evidenced in the literature.[100,129,144,145] Functional studies, especially those centered on the genes identified above and the blood brain barrier, would be of value.

We identified several genes in module M43 with translational potential. Of these, we discovered that haploinsufficiency of *Bcl11b*, *Foxp1*, *Pde10a*, and *Rgs9* led to gene expression changes that overlapped M43. Thus, hub genes of M43 can be targeted to alter the transcriptional states of striatal neurons. 17 other genes, including *Pde10a*, encode proteins that are targeted by approved small molecule drugs and 19 others, are considered targetable. Notably, Logrip and colleagues discovered that injection of TP-10, a PDE10A inhibitor, into the dorsolateral striatum of rats significantly decreased alcohol, but not sucrose, consumption.[146] Given that PDE10A is selectively expressed in striatal SPNs with little appreciable expression elsewhere in the brain, the present data further validate this gene as a potential target for pharmacotherapy in AUD that may possess relatively low side effect liability.[105,147] The validation of PDE10A as a drug target for AUD in the Logrip et al. (2015) study validates the present approach of discovering novel drug targets using snRNA-seq in mouse CIE models and warrants further investigation of the genes we prioritize in Tier 1.

When considering how to leverage the present dataset for therapeutic strategy development, biological context should be carefully considered. For instance, while logic would suggest that a decrease in expression of a gene target should be treated by functional activation of its cognate protein, the opposite is the case for *Pde10a*, which is decreased in expression in response to CIE, while inhibition of PDE10A reduces alcohol consumption.[146] Thus, a gene expression change may reflect a compensatory mechanism that may need to be enhanced for therapeutic benefit. In the case of module M43, down-regulation may be a consequence of decreased synaptic drive onto SPNs. As such, inhibiting an inhibitor of D1 dopamine receptor signaling (eg., PDE10A) may represent a logical therapeutic approach supported by data.[38,148–150]

F. Limitations and Future Directions

We note several limitations of our study. Our dataset was better powered to detect differentially expressed genes in common cell types than rare cell types. Thus, the three well-studied interneuron populations of the dorsal striatum -- including the low-threshold spiking somatostatin-expressing INs, the fast-spiking parvalbumin-expressing INs, and the tonically firing cholinergic choline acetyltransferase-expressing INs -- require deeper assessment. Larger samples would be required to detect subtle changes in these cell types. In addition, transcriptional effects of alcohol may vary across striatal sub-regions. These sub-region-specific effects could be elucidated though spatial transcriptomics. Transcriptional effects of alcohol may also vary dynamically across different phases of exposure. It will be valuable to assess these temporal patterns, comparing the CIE paradigm to other models of alcohol exposure, including models with a volitional component. Our findings lay the groundwork for functional studies to test causal roles for

differentially expressed genes and gene networks as mediators of alcohol effects on striatal circuits and related behavior. Given the concordant decrease in M43 gene expression in our snRNA-seq of mouse CIE and bulk tissue mRNA-seq of human AUD, single-cell genomic data from the dorsal striatum of humans with AUD is warranted to further validate the translational capacity of the presently identified gene targets.

CHAPTER III: PRECLINICAL EVALUATION OF AN ANTISENSE OLIGONUCLEOTIDE GENE THERAPY FOR HUNTINGTON'S DISEASE USING SINGLE CELL GENOMICS

A. Abstract

As a monogenic disorder, Huntington's disease (HD) is at the forefront for gene-therapy innovation in neurodegeneration. In particular, several approaches are being evaluated to reduce the levels of toxic huntingtin (HTT) protein in the brain. One challenge to clinical innovation is our ability to discern detailed information about how HD and its potential therapeutics impact the brain. Single-nucleus RNA sequencing is a cutting-edge technology capable of providing this level of detail. Here, we studied cell type-specific transcriptomic effects of HD mutations in the striatum of a knock-in mouse model, $HTT^{Q111/+}$. Further, we examined the cellular impacts of a non-allele specific HTT-lowering antisense oligonucleotide (ASO). We characterized substantial transcriptional effects of the HD mutation in spiny projection neurons, the cell type most vulnerable to HD neurodegeneration. Surprisingly, HTT-lowering ASO treatment exacerbated many of these transcriptional changes. Understanding these cell type-specific effects of ASO treatment could aid in the interpretation of HTT-lowering toxicity that has recently been observed in human patients.

B. Introduction

There are few disease-modifying treatments for neuropsychiatric disorders. The successes of antisense oligonucleotide (ASO) gene therapies to treat spinal muscular atrophy and Duchene muscular dystrophy have raised hopes for ASO therapies for multiple

neurological disorders. Huntington's Disease (HD) is a neurodegenerative disorder caused by a single, known gene mutation. Our knowledge of the gene mutation that causes HD make it a prime candidate for gene therapy. Several promising therapeutic candidates have progressed to clinical trials.

Huntington's Disease (HD) is a monogenic age-related neurodegenerative disease that mirrors many of the hallmark characteristics of other neurodegenerative diseases -- cognitive decline, movement dysregulation and polyneuropathy are all features of HD. The disease is caused by a trinucleotide CAG repeat on exon 1 of the HTT gene. The molecular result is a mutant HTT mRNA that contains an expanded polyglutamate tract. The mRNA is then transcribed into either a full-length mutant HTT (mHTT) or fragmented isotypes of the mHTT protein. Though this mutation permeates every cell type, the striatum is the earliest and most severely affected region. The striatum is made up of roughly 95% Spiny Projection Neurons (SPNs) and 5% interneurons. SPNs are GABAergic neurons that can be further subdivided into a "Direct" striatonigral pathway and "Indirect" striatopallidal classification scheme. Notably, Indirect SPNs (iSPNs) are affected earlier and more severely than Direct SPNs (dSPNs) in HD.[151]

The deleterious effects of HD are numerous, but many are caused by a toxic gain-of-function of mutant HTT (mHTT) operating in parallel to a loss-of-function attributed to remaining wildtype HTT (wtHTT).[152,153] One promising gene therapy approach centers on lowering HTT. RNA-induced silencing vectors (RNAi), antisense oligonucleotides (ASOs) and, more recently, small molecules designed to lower HTT have progressed to clinical trials. In the past several years, five separate gene therapy-based HD trials were halted for efficacy and safety reasons.

One of these products, Roche's promising non-allele specific, HTT-lowering ASO Tominersen, had advanced to Stage Three clinical trials when drug administration was halted in 2021.[154] Though reports shy away from labeling the trial suspension as being due to safety concerns, patients on placebo saw slower disease progression than those given the drug. This result was dose dependent, with patients given higher dosages experiencing worse outcomes.[155] The trial only included patients with clinical signs of disease, but when patients with a lesser disease burden were subset from high disease-burden patients, they did slightly better than placebo. Though it is uncertain whether this is due to chance or biological effect, Roche is currently recruiting earlier disease stage patients only for a Stage Two clinical trial of Tominersen.[156] Sources of potential toxicity in discontinued trials remain unclear. This is in part due to the difficulty in properly evaluating the impacts of potential therapeutics on the human brain.

Several studies have elucidated the complicated downstream effects of the HD mutation and we have a robust, human-HD replicated understanding of transcriptomic changes that occur in the disease process.[49,64,157,158] Here, using single-cell genomics, we evaluated the brain cell type-specific effects of a therapeutically relevant ASO gene therapy in a genetically precise knock-in mouse model of HD. 6-month-old HTT Q111/+ mice were treated chronically with a non-allele specific HTT-lowering ASO with characteristics similar to ASOs in active clinical development as HD therapeutics. HTT Q111/+ and wildtype mice injected with non-targeting ASOs, or saline were evaluated as controls. We describe substantial transcriptional effects of the HD mutation in spiny projection neurons, the cell type most vulnerable to HD neurodegeneration. Surprisingly, our HTT-lowering ASO treatment exacerbated many of these transcriptional changes. This is in

contrast with literature detailing behavioral rescue in animals treated with a similar ASO. Further study is required to pinpoint how these data make sense when taken together. One possibility arises from the pairing of mHTT and wtHTT in heterogeneous HD, producing both loss-of-function effects from the loss of wtHTT and gain-of-function effects from the gain of *m*HTT. It may be that the loss-of-function effects are more molecularly pronounced, while it is the gain-of-function effects that most contribute to clinical disease. Understanding cell type-specific effects of ASO treatment could aid in the interpretation of HTT-lowering toxicity that has recently been observed in human patients.

C. **Methods**

Animals

We used the B6.HTT Q111 mouse strain (hereafter 'Q111'; JAX strain 003456) who have a targeted mutation replacing mouse HTT exon 1 with human HTT exon 1 containing an expanded CAG tract. The average CAG length in our cohort was 114. The cohort was bred by crossing heterozygous Q111 mice (Q111/+) and WT mice to produce Q111/+ and wild-type (WT) littermates. Experiments were approved by the Western Washington University Institutional Animal Care and Use Committee under protocol 16-011.

Anti-Sense Oligonucleotide (ASO) Design

We used a previously described HTT-exon-42-targeting ASO (Ionis 444652) with sequence TTTCTCTATTGCACATTCCA. Chemically, the ASO is a 5-10-5 2'MOE (2'O-methoxyethyl) gapmer with PS backbone, except for the inner three wing nucleotides that are PO. As a control, we used an ASO with the same backbone chemistry

with no known target in the mouse genome (Ionis 676630; CCTATAGGACTATCCAGGAA). ASOs were dissolved in PBS to a final concentration of 30ug/uL and dosed with a 300ug/10uL bolus injection.

We tested the ASO on four mice, finding an average of 34% reduction in HTT expression after 8-weeks of treatment. In previous testing, plasma levels of the inflammatory marker neurofilament light (NfL) by electrochemiluminescent ELISA according to manufacturer protocol (R-PLEX Human NfL, Mesoscale Discovery; MSD) with no elevation present in any of the groups, suggesting the ASO was not causing apparent inflammation (data not shown?)

Experimental design

Our experimental design included four groups of mice: WT saline-treated, Q111/+ saline-treated, Q111/+ non-targeting ASO-treated, and Q111/+ HTT-lowering ASO-treated (Fig. 3.1). We treated four mice from each group (2M, 2F) to be processed using NextGem3 technologies, resulting in sixteen mice total.

Mice were treated with ASO or saline via two intracerebral ventricular injections at 2.5 months and 8-weeks later at 4.5 months and sacrificed at 6.5-months of age for a total ASO duration of 16-weeks. Mice were sacrificed by fatal injection of sodium pentobarbital (Fatal Plus, Covetrus). Whole brain was extracted and placed on ice for 2 minutes, followed by a microdissection to collect the striatum, cortex, and cerebellum. Tissues were placed in cryotubes and snap-frozen in liquid nitrogen followed by storage at -80C.

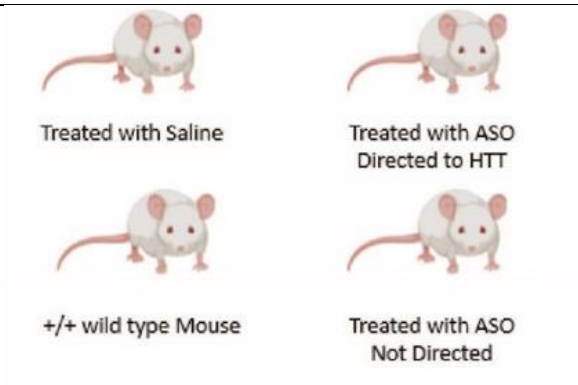

Figure 3.1. HD-ASO experimental design Our experimental design included four groups of mice: WT saline-treated, Q111/+ saline-treated, Q111/+ non-targeting ASO-treated, and Q111/+ HTT-lowering ASO-treated. We treated four mice from each group (2M, 2F) to be processed using NextGem3 technologies, resulting in sixteen mice total. Mice were treated with ASO or saline via two intracerebral ventricular injections at 2.5 months and 8-weeks later at 4.5 months and sacrificed at 6.5-months of age for a total ASO duration of 16-weeks

HTT *quantification*

HTT protein was quantified by electrochemiluminescent ELISA and read on a QuickPlex SQ120 (MSD) according to previously described methods (**). Briefly, tissues were mechanically homogenized in a non-denaturing lysis buffer and lysates were added to MSD plates coated with capture antibody and incubated for 1 hour. After washing, detection antibody was then applied for 1 hour, and finally plates were read using Read buffer B. Capture and detection antibody pairs were as follows: WT, HTT-2133 (CHDI 900002133) and D7F7-Sulfo-tag (CST mAB5656); Mutant (Q111) HTT, HTT-2B7 (CHDI-90000830) and MW1-Sulfo-tag (DSHB).

snRNA-seq data analysis

Preprocessing of the 16 mice from the 3' dataset occurred in conjunction with fourteen mice from the same experiment that had been processed to produce a 5' dataset. Genome alignment (mm10), cell calling, and read counting were performed with cellranger (v7.0.0.), We completed standard quality control (QC) and single-cell processing with Seurat.[85] We removed cells that did not meet the criteria of minimum 500 reads, minimum 250 features and a mitochondrial ratio of less than 0.20. We used SCTransform() followed by integration using anchors selected from SelectIntegrationFeatures (nfeatures = 3000). Following integration we separated the 5' and 3' datasets, working exclusively with 3' data from this point. We scaled the data and completed a standard Seurat processing and clustering protocol: principal component analysis (npcs = 30), Uniform Manifold Approximation and Projection visualization (dims: 1:30), nearest-neighbors analysis (dims = 1:30) and clustering (res = 0.1). We repeated the process of scaling through clustering four times, with each new iteration run without potentially interfering doublets that had been identified and removed in the previous round.

We used established markers for striatal cells to assign cell-types to clusters, dropping clusters with mixed markers that meet criteria for doublets: direct pathway spiny projection neurons (dSPNs; *Drd1*+), indirect pathway spiny projection neurons (iSPNs; *Drd2*+), atypical spiny projection neurons (termed "eccentric", eSPN; *Otof*+), cholinergic interneurons (IN-Chat; *Chat*+), parvalbumin interneurons (IN-PV; *Kit*+), somatostatin interneurons (IN-Sst; *Sst*+), astrocytes (*Slc1a3*+, *Rorb*+), oligodendrocytes (*Mog*+, *Aspa*+), polydendrocytes (also known as oligodendrocyte precursor cells; *Pgdfra*+, *Coll11a1*+), mural cells (*Vtn*+, *Pgdfrb*+), endothelial cells (*Flt1*+, *Slco1a4*+), ependymal

cells (*Rsph1+*), and microglia (*Cx3Cr1+*, *C1qc+*).[86] Finally, we used kmeans clustering (centers = 2) around the sex-discriminating marker *Xist* to separate male and female mice, which had been multiplexed together.

Differential expression analysis

We identified differentially expressed genes (DEGs) using the program EdgeR. We compared differential expression between six contrast groups: 1) HD-Q111 treated with saline compared to wildtype treated with saline (HD-Saline v. WT-Saline), 2) HD-Q111 treated with undirected ASO compared to HD-Q111 treated with saline (ASO-CNTL v. HD-Q111), 3) HD-Q111 treated with undirected ASO compared to WT treated with saline (ASO-CNTL v. WT-Saline), 4) HD-Q11 treated with HTT-directed ASO compared to HD-Q111 treated with saline (HD-ASO v. HD-Saline), 5) HD-Q111 treated with HTT-directed ASO compared HD-Q111 treated with undirected ASO (HD-ASO v. ASO-CNTL), 6) HD-Q111 treated with HTT-directed ASO compared to wildtype treated with saline (HD-ASO v. WT-Saline).

Validation in Independent Datasets

We used Fisher's Exact Tests to compare DEGs from our single-cell atlas of a six-month-old Q111+ HD mouse model to established literature. As there is not a single-cell database available for the HD Q111+ mouse model, we compared our SPN single-cell results to available bulk RNA-seq data.

D. **Results**

We analyzed 54,141 high-quality cells, which corresponded to marker genes associated with major striatal cell types: 22566 dSPNs, 14627 iSPNs, 1297 eSPN, 2168 *PV+*

interneurons, 892 *SST*+ interneurons, 738 *CHAT*+ interneurons, 5897 astrocytes, 1972 oligodendrocytes, 1008 endothelial cells, 483 microglial, 1005 polydendrocytes, and 816 ependymal cells (Fig. 3.2, Table S3.1).

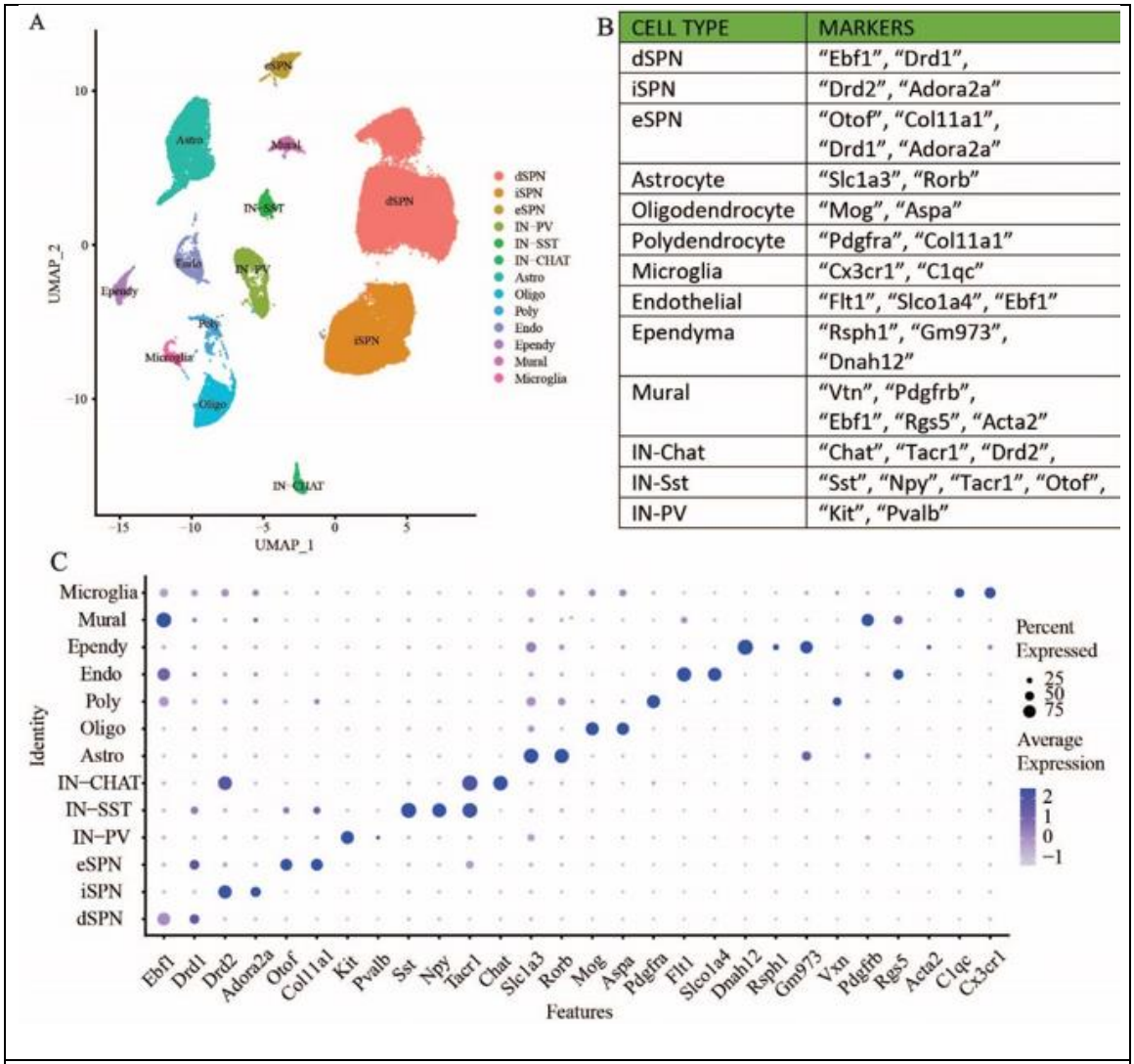

CELL TYPE	MARKERS
dSPN	"Ebf1", "Drd1",
iSPN	"Drd2", "Adora2a"
eSPN	"Otof", "Col11a1", "Drd1", "Adora2a"
Astrocyte	"Slc1a3", "Rorb"
Oligodendrocyte	"Mog", "Aspa"
Polydendrocyte	"Pdgfra", "Col11a1"
Microglia	"Cx3cr1", "C1qc"
Endothelial	"Flt1", "Slco1a4", "Ebf1"
Ependyma	"Rsph1", "Gm973", "Dnah12"
Mural	"Vtn", "Pdgfrb", "Ebf1", "Rgs5", "Acta2"
IN-Chat	"Chat", "Tacr1", "Drd2",
IN-Sst	"Sst", "Npy", "Tacr1", "Otof",
IN-PV	"Kit", "Pvalb"

Figure 3.2: snRNA-seq of the striatum from mice groups including HD-Saline, WT-Saline, HD-ASO, and ASO-Cntr. A. Uniform manifold approximation and projection (UMAP) of 54,141 cellular nuclei showing discrete clusters corresponding to 13 cell types. B. Cell type specific markers used to assign cells. C. Expression of top cell type marker genes.

These cells were spread across our experimental groups, including 11619 WT saline-treated cells, 13124 Q111 saline-treated cells, 14077 Q111 non-targeting ASO-treated, and 15321 Q111 HTT-lowering ASO-treated. Breakdown by cell type within each experimental group did not reveal notable differences (Fig. 3.3).

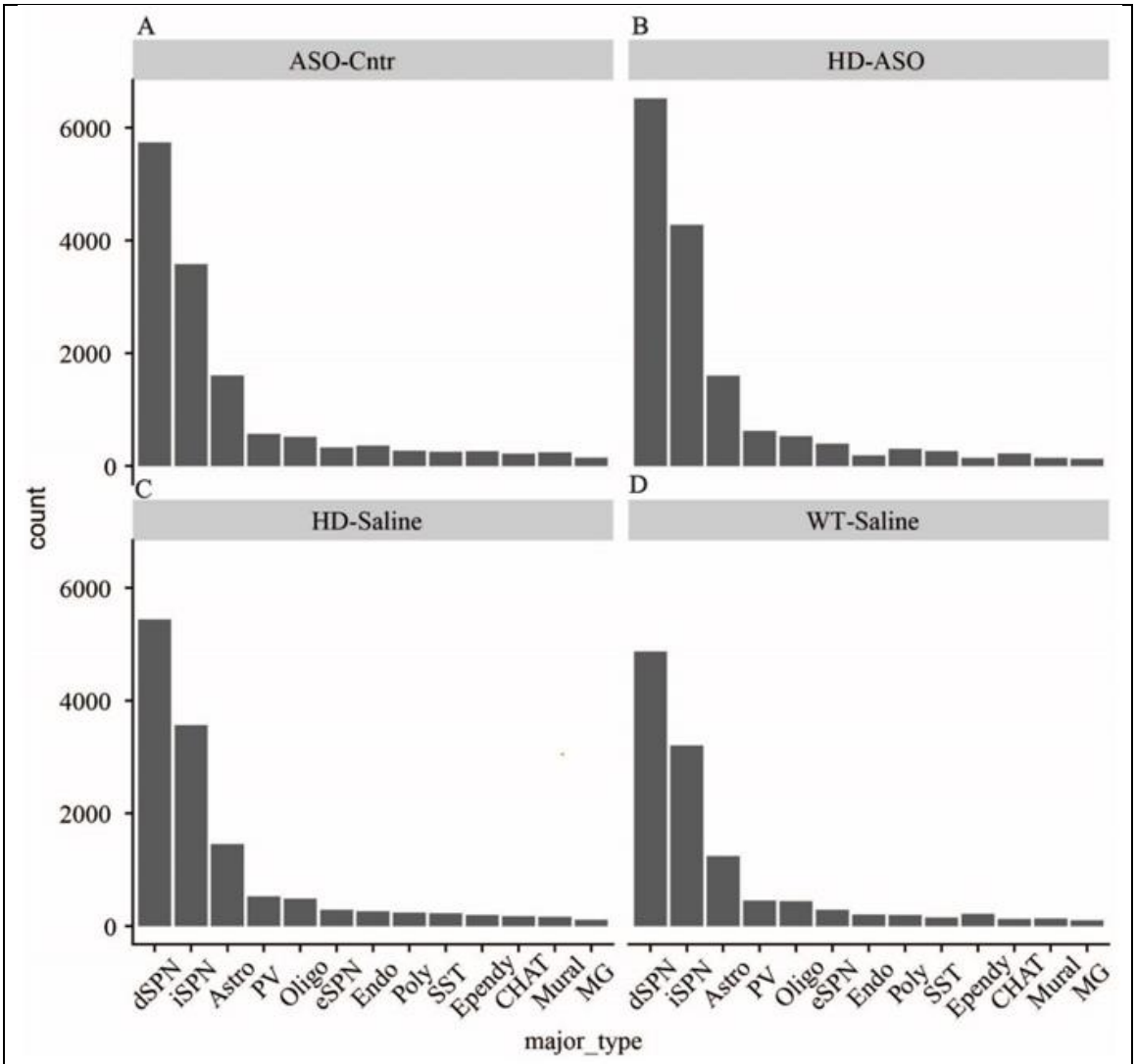

Figure 3.3: Cell counts by experimental group. A. Distribution of cell types in the ASO-Cntl group. B. Distribution of cell types in the HD-ASO group. C. Distribution of cell types in the HD-Saline group. D. Distribution of cell types in the WT-Saline group.

After filtering DEGs for expression level (pct.1 > 0.15 or pct.2 > 0.15) and statistical significance (FDR < 0.05) we identified 95,670 DEGs across the six contrasts tested. The DEGs matched what would be expected power-wise in terms of cell type specificity. We identified significant, cell-type specific variations in differential expression between our contrast groups (Fig. 3.4; Table S3.2-S3.3).

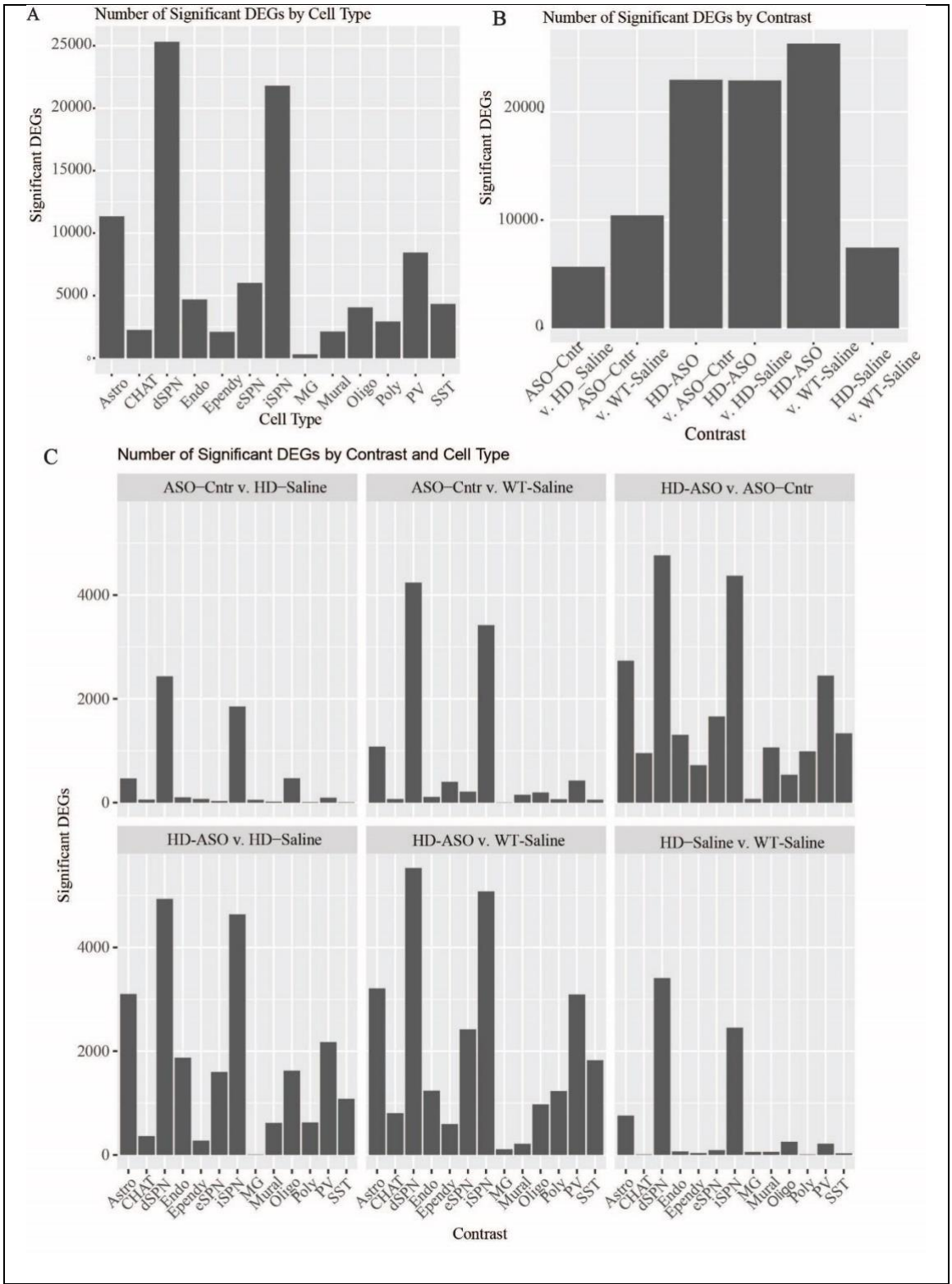

Figure 3.4: DEG distribution across cell types and contrasts. A. Distribution of DEGS by cell type across all groups. B. Distribution of DEGS by contrast group. C. Distribution of DEGs by cell type and contrast group.

Our most significant results from the single-cell genomic atlas for the effects on HD on the striatum of a Q111+ mouse model include similar dysregulation in canonical SPNs, minimal evidence of neuroinflammation, and dysregulation in vascular cell types. Results from our evaluation of an HTT-lowering ASO gene therapy indicate an exacerbation of the early HD signature in response to allele-nonspecific ASO therapy with only minimal signs of rescue.

Single-cell genomic atlas for the effects of HD on the striatum of a Q111+ Mouse Model

We characterized the HD signature in 6-month-old Q111 mice by analyzing single-cell genomic data from the contrast: HD-Saline v. WT-Saline. Our atlas includes 24,743 quality cells distributed between the two groups with 13,124 in the HD-Saline group and 11,619 in the WT-Saline group. We identified 7439 cell type specific DEGs with the following cellular distribution: 3408 dSPNs, 2451 iSPNs, 90 eSPNs, 755 Astrocytes, 56 microglial, 252 oligodendrocytes, 37 ependymal, 65 endothelial, 216 *PV*+ interneurons, 31 *SST*+ interneurons, 9 *CHAT*+ interneurons, 10 Polydendrocytes, and 59 mural cells. Our cell type specific findings are aligned with what would be expected from the literature. The signature at this age and CAG-repeat length is subtle, but observable, at this early time point (Fig. 3.5). We performed Gene Ontology (GO) term analysis on several cell types to identify biological relevance of DEGs (Table S3.4).

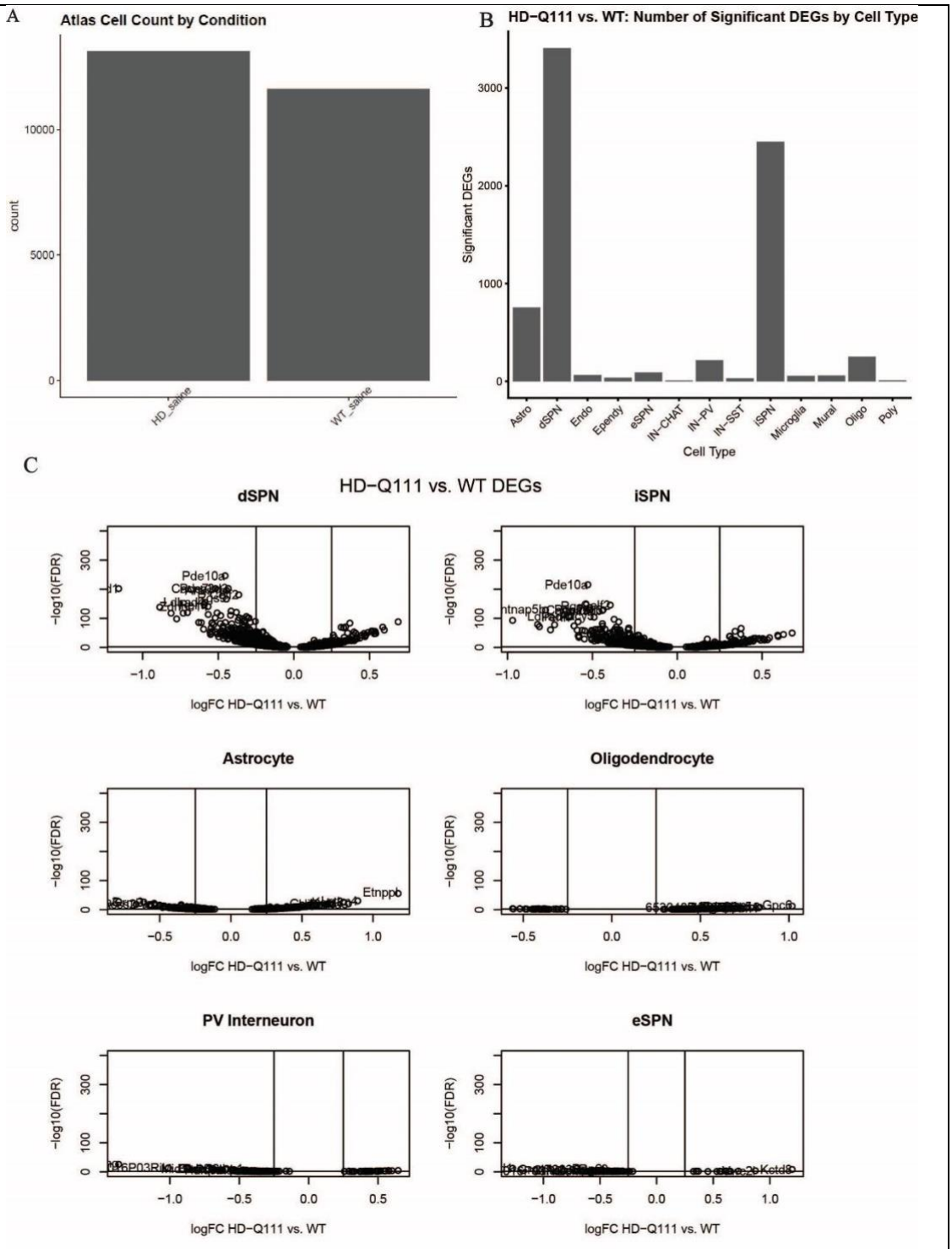

Figure 3.5: HD-Q111+ atlas DEG characteristics. A. Cell count by Atlas group. B. Distribution of DEGS by cell type. C. Volcano plots from the six cell types with the highest number of DEGs.

Canonical Spiny Projection Neurons Exhibit Similar Patterns of Dysregulation

Of the 3408 significant (FDR<0.05) dSPN DEGs identified, 788 were upregulated and 2620 were downregulated. The upregulated genes were enriched for GO terms involved in metabolism. Top GO terms included biosynthetic process, respiratory electron transport chain, cellular metabolic process, and ATP metabolic process. The downregulated genes were enriched for GO terms involved in transport, cellular survival, and cell communication. Top terms included vesicle-mediated transport to the plasma membrane, negative regulation of transport, protein localization to organelle, regulation of cell death and regulation of cell growth.

Of the 2451 significant (FDR<0.05) iSPN DEGs identified, 618 were upregulated and 1833 were downregulated. The upregulated genes were enriched for GO terms involved in biosynthetic processes, metabolic processes, and translation. Top terms include organonitrogen compound biosynthetic process, cellular amide metabolic process, and cytoplasmic translation. The downregulated genes were enriched for GO terms involved synaptic processes, signaling, and morphogenesis. Top terms included protein localization to synapse, positive regulation of cell morphogenesis involved in differentiation, regulation of glutamate receptor signaling pathway and regulation of dendritic spine morphogenesis.

To look more closely at the differences in gene expression changes between dSPNs and iSPNs, we next identified those genes that were unique to each subtype compared to the other projection neuron. Most DEGs were common to both SPNs. Between 788 upregulated dSPN DEGs and 618 upregulated iSPN DEGs, 457 are held in common. This amounts to 74 percent of iSPN upregulated genes being shared with dSPN genes. Across

2620 downregulated dSPN DEGs and 1833 downregulated iSPN DEGs, 1601 were held in common. This amounts to 87 percent of iSPN down regulated genes being shared with dSPN genes.

Previous work in the Q175 mouse model at 6-months of age hypothesized that mtRNA release from iSPNs, associated with a cell type specific loss of functionality in OXPHOS pathway genes, contribute to an innate immune response that may account for the cell type's vulnerability.[65] To examine this possibility within our dataset we compared percentage of mitochondrial genes between cell types, finding similar levels of mtRNA between iSPNs and dSPNs. It may be that these are signs of iSPN vulnerability that are not seen as early in our Q111 model.

Evidence of Neuroinflammation is Limited

Of the 56 significant microglia DEGs, 52 genes were upregulated, and 4 genes were downregulated. Upregulated genes were enriched for GO terms involving metabolism and translation with top terms including cytoplasmic translation, amide biosynthetic process, translation, and peptide biosynthetic process. Though we did not see a plethora of classic microglia-associated inflammation markers, the DEGs do suggest an enhanced metabolic state of heightened activity in the HD Q111 mouse model. Several genes also suggest an inflammatory state: IL1RAP is involved in signaling upstream of interleukin 1-responsive genes (logFC = 1.026, FDR = 0.013) and LRRC19 is an upstream positive regulator of the pro-inflammatory NIK/NF-kappaB signaling cascade (logFC = 1.053, FDR = 0.0135).

Of the 755 significant astrocyte DEGs, 367 genes were upregulated, and 388 genes were downregulated. Upregulated genes were enriched for GO terms involving signaling and translation. Top terms include regulation of trans-synaptic signaling, cognition, ribosomal small subunit biogenesis and regulation of membrane potential. Downregulated genes were enriched for GO terms associated with bidirectional regulation of metabolic and biological processes. Top terms include regulation of nitrogen compound metabolic process, positive regulation of multicellular organismal process, negative regulation of metabolic process and positive regulation of macromolecule metabolic process.

Previous work has identified distinct states of Astrocyte activation in HD.[159] We re-clustered astrocytes by known reactive markers, comparing the number of reactive astrocytes in the WT versus HD-Q111 mice. We did not find evidence of increased reactivity in the HD-Q111 astrocytes when compared to WT.

Evidence of Dysregulation in Vascular Cell Types

We identified 65 significant endothelial DEGs including 41 upregulated genes and 24 downregulated genes. Upregulated genes were not enriched for any GO terms with top DEGS including *Cd200*, *Dbp*, *Luzp2*, and *Mgp*. Downregulated genes were enriched for three GO terms: regulation of ERK1 and ERK2 cascade, cellular response to laminar fluid shear stress and response to laminar fluid shear stress.

We identified 37 ependymal DEGs, including 11 upregulated and 26 downregulated genes. Downregulated genes returned GO terms associated with negative regulation of cholesterol metabolic and biosynthetic processes. Top downregulated genes included *Stat1*, *Ddx60*, and *Bcl1*. *Apoe* was also among the significantly downregulated genes.

Upregulated genes did not return any significant GO terms. Top DEGs included *Il1rapl2, and Lrrtm4*. Other notable upregulated genes included the adhesion proteins cadherin 12 (*Cdh12*) and 19 (*Cdh19*).

Atlas Validation in an Independent Dataset

Our top DEGs in the dSPN and iSPN cell types, where our data is best powered given that these are the most common cells of the striatum and also where the HD signature is most pronounced, are statistically associated with HD DEGs identified in previous studies.[64] We computed Fisher's Exact Tests on several contrasts between our DEGs and the HD DEGs identified in the seminal Langfelder to identify significant associations. Downregulated dSPN genes from our study were associated with downregulated genes from the Langfelder study (OR = 3.43, p = 2.2e-16), as were upregulated dSPN genes associated with upregulated genes from the Langfelder study (OR = 2.12, p = 4.4e-14). Downregulated iSPN genes from our study were associated with downregulated genes from the Langfelder study (OR = 5.04, p = 2.2e-16) and upregulated iSPN genes from our study were associated with upregulated genes from the Langfelder study (OR = 2.57, p = 2.2e-16). Of note, Pde10 is a key marker of early HD progression and emerged as the top DEG for both iSPN and dSPN cell types.[160]

HTT-lowering ASO treatment caused exacerbation of the HD-associated transcriptomic dysregulation

We first confirmed that the ASO had knocked down HTT by looking at HTT expression across our contrast groups. As expected, only the contrast groups that included the ASO – HD-ASO group – exhibited downregulated HTT (Fig. 3.8).

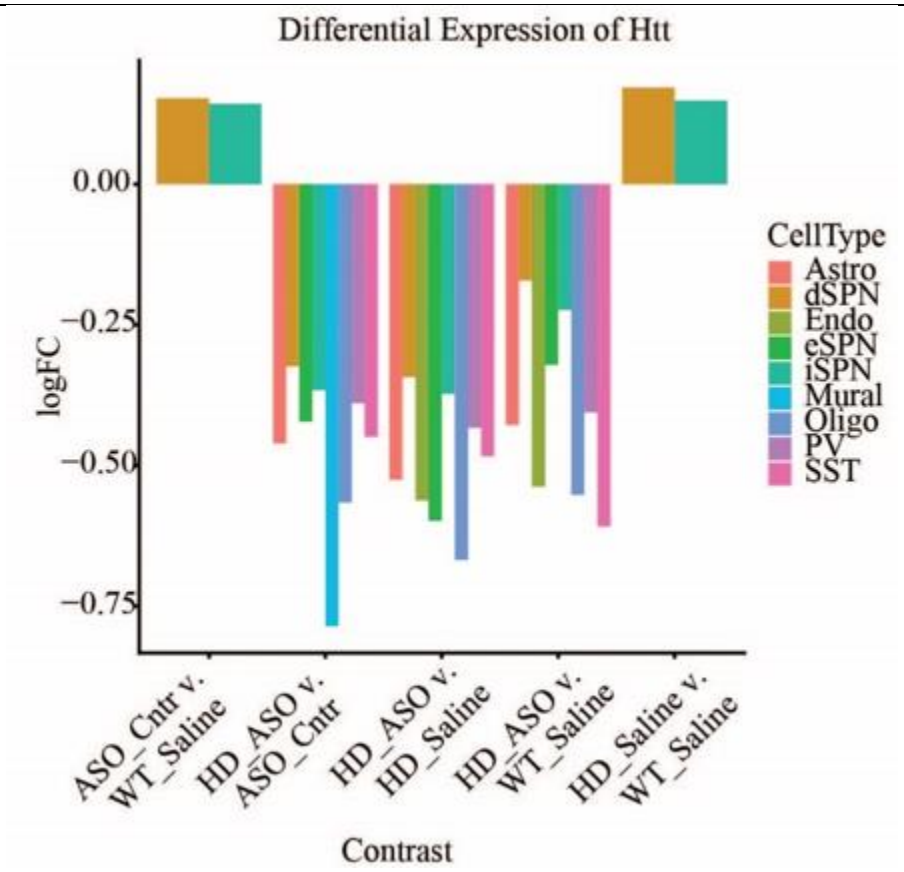

Figure 3.6: Differential expression of HTT by contrast.

Having already examined the baseline HD-Q111 signature compared to WT (HD-Saline vs. WT-Saline contrast) as our Atlas, we next wanted to look at how the ASO impacted our HD-Q111+ mouse. If our directed ASO had successfully resulted in a rescue we would expect the ASO-treated group to have become more similar to WT.

Comparing the contrast HD-ASO vs. ASO-Cntr to the contrast HD-Saline vs. WT-Saline (ASO treatment biplot), we instead found that the treatment had largely exacerbated the HD signature in canonical SPNs, with comparatively little evidence of rescue (Fig. 3.7). This pattern of exacerbation was seen in the majority of cells that returned a statistically

significant signature, with astrocytes and oligodendrocytes also exhibiting subtle evidence of rescue.

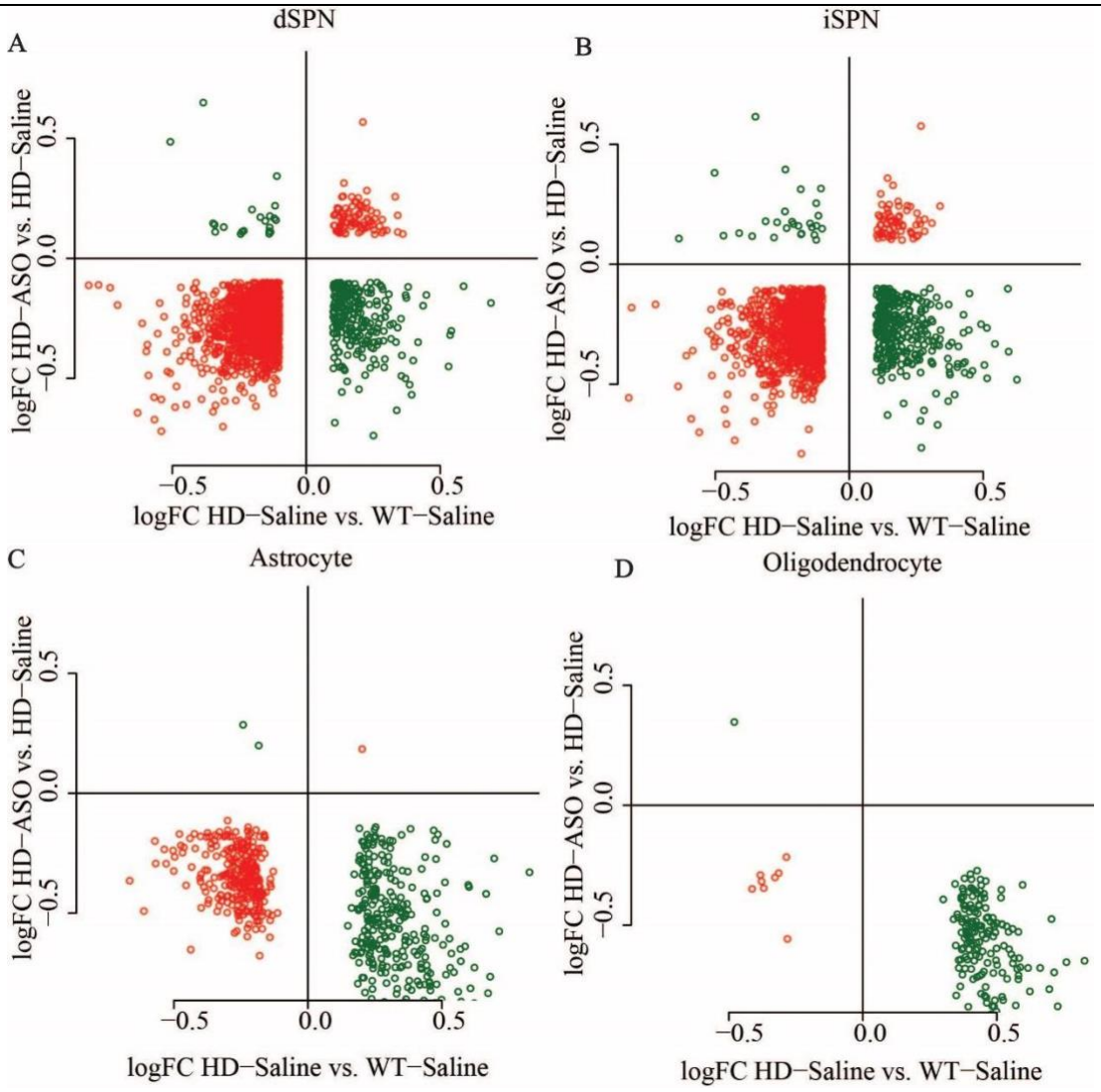

Figure 3.7: ASO treatment exacerbates HD-Signature with limited rescue. A. Biplot comparing dSPN HD-Saline vs. WT-Saline and ASO-Cntr vs. HD-Saline. B. Biplot comparing iSPN HD-Saline vs. WT-Saline and ASO-Cntr vs. HD-Saline. C. Biplot comparing oligodendrocytes between HD-Saline vs. WT-Saline and ASO-Cntr vs. HD-Saline. D. Biplot comparing astrocytes between HD-Saline vs. WT-Saline and ASO-Cntr vs. HD-Saline.

Following this surprising result, we wanted to know whether the undirected ASO played a role in HD-signature exacerbation. We addressed this possibility by analyzing DEGs

from the contrast ASO-Cntr v. HD-Saline. Limited differential expression between these two groups would indicate that the undirected ASO has a limited impact on the HD signature. To the extent that there is differential expression between these groups, this may indicate an effect of the undirected ASO independent from the HD-targeted therapy itself.

Filtering for (pct.1 > 0.15 | pct.2 > 0.15) & FDR < 0.05, we identified 5663 cell type specific DEGs with the following cellular distribution: 2433 dSPNs, 1853 iSPNs, 31 eSPNs, 466 Astrocytes, 54 microglial, 470 oligodendrocytes, 70 ependymal, 102 endothelial, 0 *PV*+ interneurons, 0 *SST*+ interneurons, 0 *CHAT*+ interneurons, 10 Polydendrocytes, and 18 mural cells (Table S3.2, Contrast AC)

To examine whether the changes in gene expression in the undirected ASO exacerbated the HD-signature we plotted a biplot comparing the HD-saline vs. WT-saline group to the ASO-Cntl vs. HD-Saline group. We found that the signature imposed by the undirected ASO did not create a pattern resembling the HD signature. This implies that, although the undirected ASO did result in dysregulated transcriptomics, it was the HTT lowering treatment itself that caused HD signature exacerbation (Fig. 3.8).

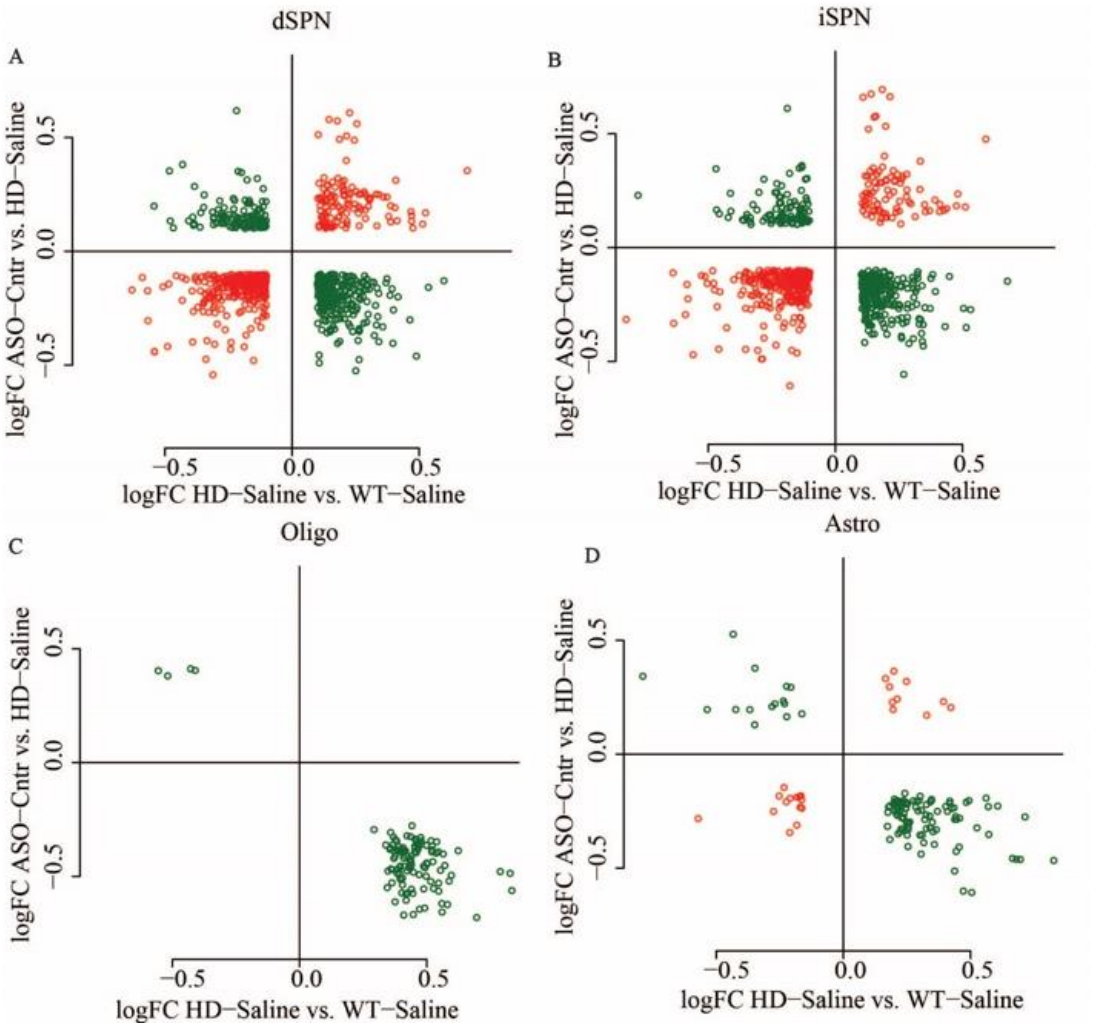

Figure 3.11: Undirected ASO does not exacerbate HD-signature. A. Biplot comparing dSPN HD-Saline vs. WT-Saline and ASO-Cntr vs. HD-Saline. B. Biplot comparing iSPN HD-Saline vs. WT-Saline and ASO-Cntr vs. HD-Saline. C. Biplot comparing oligodendrocytes between HD-Saline vs. WT-Saline and ASO-Cntr vs. HD-Saline. D. Biplot comparing astrocytes between HD-Saline vs. WT-Saline and ASO-Cntr vs. HD-Saline.

To identify which pathways as associated with the strong exacerbation signal and which are associated with more subtle signs of rescue, we performed GO analysis on the genes within each ASO treatment biplot quadrant for dSPNs, astrocytes, and oligodendrocytes (Table S3.4, S3.5).

First, we asked whether the exacerbation signature could be attuned to specific biological significance. A GO term analysis of dSPN Q2 genes (n=87) returned 79 GO terms enriched for terms involving metabolism, ribosomes, and translation. An analysis of Q3 genes (n=1589) revealed 1514 terms, including a wide range of biological processes. This analysis indicates that a great variety of biological processes have been impacted by the HD signal exacerbation, rendering a specific finding unlikely.

We next asked whether the genes rescued in the ASO treatment group (Q1, Q4) were biologically significant, focusing again on dSPNs. A GO term analysis of Q1 genes (n=21) did not return any GO terms. Analysis of Q4 genes (n=251) returned 116 terms. Top terms involved neurogenesis with further enrichment in cell migration and signaling terms.

We were also interested in the moderate rescue in astrocytes and oligodendrocytes. For these cell types we centered our analysis on Q4. These are genes that are in HD when compared to WT, but then downregulated by our ASO. Astrocytes show 294 genes in Q4, which return 271 GO terms. Top terms involved synaptic regulation, generation of neurons, and signaling. Oligodendrocytes show 165 genes in Q4 Top terms include generation of neurons, nervous system development, cell-cell adhesion, and positive regulation of cell projection organization.

E. **Discussion**

In this study we have characterized the transcriptional signature of a 6-month-old HD-Q111 mouse model and assessed transcriptional changes following HTT-lowering ASO treatment. Key findings in our characterization of a 6-month-old HD-Q111 mouse model

include (1) similar patterns of dysregulation in canonical SPNs, (2) limited evidence of neuroinflammation, and (3) dysregulation in vascular cell types. The key finding from our treatment of the HD-Q111 mouse model with an HTT-lowering ASO treatment was exacerbation of the HD-associated transcriptomic dysregulation.

Similar Patterns of Dysregulation in Canonical SPNs

We saw fewer DEGs in iSPNs than in dSPNs, with the overwhelming majority of these genes, 74 percent of upregulated genes and 87 percent of downregulated genes, shared between these two canonical SPN cell types. It is somewhat surprising that we found a greater number of significant transcriptional changes in dSPN cells than in iSPN cells because iSPNs are the cell type most vulnerable to the HTT mutation. This is evidenced by the fact that iSPNs are the first cells to experience cell death in the human striatum. Knock-in mouse models have been shown to exhibit this differential vulnerability pattern. In the Q140 knock-in mouse model differential expression of the D1 and D2 markers that differentiate dSPNs from iSPNs show a 15 percent reduction in D2 markers as early as two months old via Western Blot, with a 20% reduction by six-months-old.[161,162] Drd2, the gene associated with the D2 receptor, is not among the significantly differentially expressed genes in this study. Other studies have noted a reduction in ENK, an iSPN-associated gene, in the Q175 knock in model, which our study also fails to replicate.[162,163] The most likely explanation is that the six-month time point is too early to see these differences in Q111 mouse model, given its shorter CAG repeat when compared to the relevant literature. This is an interesting result because it suggests that other changes predicate iSPN-specific vulnerability. It may be that these events are not causal, and the vulnerability is specific to the mHTT itself, but it may alternatively be that molecular

events downstream of mHTT itself are the cause of iSPN vulnerability. This may open possibilities for therapeutics downstream that could have a disease-modifying impact.

Limited Evidence of Neuroinflammation

Neuroinflammation is a known HD phenomenon with evidence of an innate immune response facilitated by inflammatory mediators, macrophages, and astrocytes. Nuclear transcription factor-κB (NF-κB) is a key regulatory of inflammatory responses. IL1RAP and LRRC19 are inflammatory mediators upregulated in the microglia population from six-month old HD-Q111+ mouse model. L1RAP is involved in signaling upstream of interleukin 1-responsive genes and LRRC19 is an upstream positive regulator of the pro-inflammatory NIK/ NF-κB signaling cascade. Both of these mediators, though significantly upregulated, showed only a small fold-change increase. We did not see upregulation in NF-κB.

Reactive astrocytes in mouse studies exhibit a correlation with disease severity. This phenomenon leads to dysfunction of glutamine transporters and downregulation of Dopamine and adenosine 3′,5′-monophosphate-regulated phosphoprotein (32 kDa) (DARPP-32) and NMDAR-NR2B subunits in SPNs. Reactive astrocyte have also been identified in human studies, with astrocytes growing in number and activation in stages 2-5 of a 0-5 scale. This supports our data from the Q111 mouse model at 6-months. Astrocytes in our study had not grown in number and did not exhibit signs of reactive gliosis. The astrocyte-specific changes that were observed in this study indicate an early stage increase in signaling and translation that may support future reactive processes.

Our limited evidence of upregulation in inflammatory mediators and lack of a definable inflammatory signature in microglia or astrocytes suggests that neuroinflammation has not yet ramped up in the HD-Q111 mouse model at 6-months-old. Given the relatively low CAG repeat length for the mouse model and its young age this evidence supports the hypothesis that neuroinflammation, though present before clinical symptoms arise, are not an early feature of the HD signature.

Evidence of Dysregulation in Vascular Cells

Endothelial cells line blood and lymphatic vessels to create a dynamic system of barriers which makes up the blood-brain barrier. HD is associated with microvascular abnormalities including increased density and compromised barrier function.[164,165]

We identified 65 significant endothelial DEGs including 41 upregulated genes and 24 downregulated genes. Upregulated genes were not enriched for any GO terms. Downregulated genes were enriched for three GO terms: regulation of ERK1 and ERK2 cascade, cellular response to laminar fluid shear stress and response to laminar fluid shear stress. Associated genes include *Akap12*, *Dusp1*, *Jun*, *Kdr*, *Klf3* and *Klf2*.

Ependymal cells line the ventricles and maintain brain homeostasis via the blood–cerebrospinal fluid barrier. This rare cell type is poorly characterized in the context of HD, which renders our results interesting even though they are sparse.[166] A notable feature from our dataset was the downregulation of immune responses in ependymal cells. *Stat1*, a gene significantly downregulated in ependymal cells, is classically an immune transcription factor. Some evidence suggests that *Stat1* deficiency can impair ependymal cell integrity and result in hydrocephalus, a finding seen in HD model

mice.[167–170] The interplay between hydrocephalus and HD in humans is unclear with only a few isolated accounts of lumbar puncture relieving hydrocephalus and lessening symptoms of chorea in HD patients.[171–173] Notably, one patient experienced hydrocephalus as a complication in the recent Tominersen ASO therapy clinical trials and several patients have experienced this complication with the ASO Nusinersen approved for use in spinal muscular atrophy.[174] This may be related to the fact that *Cdh12* and *Cdh19*, cadherin-associated genes involved in the formation and maintenance of cellular junctions and adhesions, were also found to be upregulated in ependymal cells.[175,176] Upregulation of these genes may cause dysregulation at the CSF-brain barrier, or may be a response to insult at this barrier.

HTT-Lowering ASO caused exacerbation of the HD Signature with limited rescue

We were surprised to find that the HTT-directed ASO treatment resulted in an exacerbation of the HD signature, with only limited evidence of rescue. This appears to be at odds with clinical data from a similar HTT-lowering ASO showing restoration of cognitive function in an HD mouse model.[177] There are several possible explanations for this result. (1) The genes in which the HD signature was exacerbated, though more plentiful, are less biologically important than those that were rescued. This would explain why one might see an exacerbated molecular signature alongside improved behavioral results. (2) Our particular ASO, which is different from the one used to produce positive pre-clinical, behavioral results in mice, has different off target effects and would not result in behavioral rescue.

In either scenario, the exacerbation of the HD molecular signature by a treatment that lowers HTT is an interesting result. Given that this ASO lowers both mutant and wild-

type HTT, it stands to reason that the molecular signature of disease is more representative of lost-of-function than gain-of-function. This is not to imply that loss-of-function consequences of this mutation are necessarily responsible for the clinical and behavioral findings of disease. It may be that although the loss-of-function signature predominates the molecular landscape, it is the more molecularly subtle gain-of-function attributes of *m*HTT that predominantly cause disease. This would also explain why we could see a molecular exacerbation while also witnessing behavioral and cognitive rescue. Perhaps we are indeed lowering the gain-of-function harm being produced by *m*HTT even while we see greater molecular evidence of the increased loss-of-function caused by knocking-down wild-type HTT.

An examination of the rescue-specific quadrant genes and GO terms points to several gene enrichments that may be associated with this gain-of-function. In particular, GO terms indicate a rescue in neurogeneration, projection and signaling. Further evaluation of the role played by each of the 251 genes in this quadrant may be fruitful. The emphasis on genes involved in neurogeneration may infer a change in neuroplasticity genes, which may in turn be related to dysregulation of Polycomb Repressive Complex 2, as has been previously reported in the HD literature.[158]

It is important to note that the purpose of these and other mouse model studies is to inform clinical decisions with an aim toward human therapeutic development. Behavioral rescues in pre-clinical mouse studies are only useful insofar as they translate to the human condition. That pan-HD ASO have thus far failed in a large clinical trial suggests that the promising behavioral rescue in a pre-clinical mouse model was not indicative of improved clinical outcomes.[73] Part of the impetus of this study was the result that

Roche's Tominersen might be clinically effective in younger patients with a lower CAG repeat length. A more positive result from this mouse model – a model in which treatment was started early and in which the CAG burden in comparatively low – would have supported this hypothesis.

F. **Limitations and Future Directions**

In this study we have presented a striatal single-cell genomic atlas of the HD-Q111 mouse model, briefly touching upon several interesting cell-type specific results including and also presented an evaluation of a pre-clinical HTT-lowering gene therapy. As a resource dataset, limitations of our Atlas include (1) potential normalization issues with the statistical approach (2) the use of a clonal animal model, (3) power in rare cell types, and (4) the challenges of reproducibility given there are not currently equivalent datasets that examine single-cell HD-Q111 transcriptional changes at six-months.

Here we have used a single-cell statistical approach that was standardized and used across the field when we began this analysis. We are observing that there is imbalance in the volcano plots where we are mostly seeing downregulated genes. This may reflect issues with the statistical analysis and potential fixes could include additional layers of normalization or using pseudobulk analysis. When we began this analysis, conventional wisdom had asserted that though the single-cell analysis approach may be overly liberal, the pseudobulk approach was overly conservative and masked important biological findings from single-cell data. Since then, there has been a slow but steady move toward the more conservative pseudobulk statistical analysis. In using pseudobulk analysis in our own work, we have noticed that the skewed volcano plots potentially indicative of

normalization issues are less prevalent when using these techniques. We plan to include a pseudobulk-based rendition of this analysis before publication.

The use of animal models, though necessary, is challenged by the translation of results from animal to human. The design and robust literature surrounding HTT knock-in mice alleviate this concern somewhat, but a robust human dataset would be preferred if possible. A common problem with single-cell datasets is the scarcity of data, which can lead to underpowered results. We have presented an Atlas with an impressive number of cells and FDR statistics that allow us to determine cell type specific signals in many cell types, but the signals would be more robust in rarer cell types with a larger dataset that produces greater statistical power. Finally, we have attempted to show replication in our dataset by comparing our data to bulk-RNA seq data because there are no equivalent single-cell datasets available. This is robust for SPNs, the cell type with the strongest signal of transcriptional dysregulation across experiments, because these changes are most likely to be observed in bulk RNA-seq data. Lesser cell types, however, cannot be validated by a bulk RNA-seq dataset as their signal is likely to be lost among the more abundant cells.

Our evaluation of a pre-clinical HTT-lowering ASO gene therapy treatment resulted in a surprising exacerbation of the HD. The major limitation of this study is a lack of behavioral assays to determine whether the ASO had a positive clinical outcome. Future studies should include both molecular and behavioral assays.

Future directions might look into the striatal cell-type specific changes we have identified in the six-month-old HD-Q111 mouse and compare these changes to other mouse models. Being able to compare this CAG-repeat length to other mouse models at six-

months-old would help to elucidate which effects of the HD signature are robust across models and which may be particular, and thus less generalizable. In terms of pre-clinical ASO evaluation, the clearest future direction would be to repeat this experiment with several other ASO vehicles and also with robust behavioral and cognitive assays. Our results taken alongside the cognitive rescue seen in a similar ASO treatment indicate that HTT-lowering gene therapy may be worthy of pursuit, even if we see exacerbation of the HD molecular signature.[178]

CHAPTER V: SUMMARY AND IMPLICATIONS OF THE RESEARCH

A. Main findings

The main findings of this study include: (1) striatal cells are dysregulated in AUD with changes seen predominantly in SPNs, (2) striatal cells are dysregulated in the HTT-Q111 mouse model as early as six-months-old (3) single-cell genomic strategies contribute to our understanding of gene therapy efficacy, especially when taken into consideration alongside functional assays.

Transcriptional Dysregulation in AUD and HD

As the most prominent cell type in the striatum, it is expected that changes in SPNs will be more statistically powerful than less common cells. This was the case in both the AUD and the HD dataset.

The AUD dataset revealed downregulation in a wide range of genes with neuron-specific functions including transmembrane receptor protein tyrosine kinase signaling pathway, including the BDNF receptor *Ntrk2,* the calcium signaling pathway, axon guidance genes (e.g., *Sema6a*) and, finally, components of voltage-gated calcium channels (*Cacnb2, Cacna2d3*), glutamate receptors (*Grid2, Grm5, Gria3*), and the cAMP signaling cascade (e.g., *Pde10a, Pde7b, Adcy5, Rgs9*).

The HD dataset also revealed significant downregulation in canonical SPNs with downregulated genes enriched for processes involving transport, cellular survival, and cell communication. Top terms included vesicle-mediated transport to the plasma membrane, negative regulation of transport, protein localization to organelle, regulation of cell death and regulation of cell growth. Several of the specific genes identified as

significantly downregulated in AUD are also dysregulated in this early model of HD. Key downregulated genes exhibiting downregulation of similar pathways in both datasets include *Ntrk2, Cacna2d3, Grm3, Gria3, Pde10a, Pde7b, Adcy5,* and *Rgs9.*

In spite of the parallels in canonical SPNs, we did not see parallels in our other findings. Though we saw evidence of neuroinflammation in our AUD dataset, evidence of a pattern of neuroinflammation in HD was lacking. Given that neuroinflammation has been shown to be a feature of HD in other datasets, we posit that the lower CAG length of 111 and the younger age at six-months have produced a model that has not yet experienced neuroinflammation. It may be interesting to compare our AUD neuroinflammatory signature to HD models with longer CAG lengths or older age to compare these signatures.

We saw some evidence of vascular cell dysregulation in both the AUD and HD atlases. In the AUD atlas key dysregulated genes in endothelial cells included downregulation of genes involved in angiogenesis. Evidence of dysregulation in HD was limited to genes associated with the sheer response and downregulation of the neuronal immune response, specifically as documented through downregulation of *Stat1*.

Single-cell Genomic Assays in Gene Therapy Evaluation

Beyond the production of single-cell transcriptional atlases as a scientific resource, we also used our HD atlas to test the efficacy of a gene therapy product. Here we have presented an HTT-lowering ASO gene therapy analysis on the Q111 mouse model. We have seen an exacerbation of the HD signature in canonical SPNs, even though a similar ASO product resulted in behavioral rescue. Two possible interpretations include (1) the

genes rescued by the ASO are responsible for the behavioral rescue, or (2) our ASO would not result in a behavioral rescue. This result highlights the importance of pairing genomic gene therapy evaluation assays with behavioral assays, which would provide a more completely picture of the therapeutic effects. Even without a paired behavioral assay, the signal of exacerbation is an interesting result as it indicates that the transcriptional dysregulation seen in HD is predominantly attributed to a loss-of-function in HTT. Our findings point more broadly to the benefits to be realized by applying single-cell genomic assays in gene therapy evaluation.

B. Strengths, limitations, and future directions

The strengths of this study include the development of two novel single-cell atlases for use in support of future research in the AUD and HD fields, our ability to look at two neuropsychiatric diseases with some shared clinical features at the single-cell level, and as an example of how single-cell genomics can be used to evaluate pre-clinical gene therapy.

In addition to the strengths and limitations identified in each study individually, an important limitation of the study as a whole is our use of animal models when our ultimate aim is to evaluate and treat human disease. This study serves as a blueprint for how a human-based genomic study might serve to answer similar questions. We have also addressed this limitation, where possible, by comparing our results to human dataset from the dorsal striatum. Given the challenges of procuring appropriate human samples and the limitations associated with human experimental design, the use of animal models remains a useful model for the study of human disease.

This study highlights the importance of understanding cell-type specific changes in neuropsychiatric disease. Contrasting and comparing the cell-type specific changes associated with neuropsychiatric disease that share common clinical characteristics is an exciting future direction in the field. The combination of increasingly sophisticated technology and novel, molecularly informed ways of thinking about neuropsychiatric disease have the potential to revolutionize how we classify and treat these diseases.

References

1. Belin, D., Jonkman, S., Dickinson, A., Robbins, T. W. & Everitt, B. J. Parallel and interactive learning processes within the basal ganglia: relevance for the understanding of addiction. *Behav. Brain Res.* **199**, 89–102 (2009).
2. Mancini, A., Ghiglieri, V., Parnetti, L., Calabresi, P. & Di Filippo, M. Neuro-Immune Cross-Talk in the Striatum: From Basal Ganglia Physiology to Circuit Dysfunction. *Front. Immunol.* **12**, (2021).
3. Gerfen, C. R. & Surmeier, D. J. Modulation of striatal projection systems by dopamine. *Annu. Rev. Neurosci.* **34**, 441–466 (2011).
4. Gokce, O. *et al.* Cellular Taxonomy of the Mouse Striatum as Revealed by Single-Cell RNA-Seq. *Cell Rep.* **16**, 1126–1137 (2016).
5. Saunders, A. *et al.* Molecular Diversity and Specializations among the Cells of the Adult Mouse Brain. *Cell* **174**, 1015-1030.e16 (2018).
6. Fieblinger, T. Striatal Control of Movement: A Role for New Neuronal (Sub-) Populations? *Front. Hum. Neurosci.* **15**, 697284 (2021).
7. Kawaguchi, Y. Physiological, morphological, and histochemical characterization of three classes of interneurons in rat neostriatum. *J. Neurosci.* **13**, 4908–4923 (1993).
8. Ibáñez-Sandoval, O. *et al.* A Novel Functionally Distinct Subtype of Striatal Neuropeptide Y Interneuron. *J. Neurosci.* **31**, 16757–16769 (2011).
9. Gentet, L. J. *et al.* Unique functional properties of somatostatin-expressing GABAergic neurons in mouse barrel cortex. *Nat. Neurosci.* **15**, 607–612 (2012).

10. Lopez-Huerta, V. G., Tecuapetla, F., Guzman, J. N., Bargas, J. & Galarraga, E. Presynaptic modulation by somatostatin in the neostriatum. *Neurochem. Res.* **33**, 1452–1458 (2008).

11. Cannizzaro, C., Tel, B. C., Rose, S., Zeng, B.-Y. & Jenner, P. Increased neuropeptide Y mRNA expression in striatum in Parkinson's disease. *Brain Res. Mol. Brain Res.* **110**, 169–176 (2003).

12. Cattaneo, S., Ripamonti, M., Bedogni, F., Sessa, A. & Taverna, S. Somatostatin-Expressing Interneurons Co-Release GABA and Glutamate onto Different Postsynaptic Targets in the Striatum. 566984 Preprint at https://doi.org/10.1101/566984 (2019).

13. Tepper, J. M., Tecuapetla, F., Koós, T. & Ibáñez-Sandoval, O. Heterogeneity and Diversity of Striatal GABAergic Interneurons. *Front. Neuroanat.* **4**, 150 (2010).

14. Mallet, N., Le Moine, C., Charpier, S. & Gonon, F. Feedforward inhibition of projection neurons by fast-spiking GABA interneurons in the rat striatum in vivo. *J. Neurosci. Off. J. Soc. Neurosci.* **25**, 3857–3869 (2005).

15. Lee, K. *et al.* Parvalbumin Interneurons Modulate Striatal Output and Enhance Performance during Associative Learning. *Neuron* **93**, 1451-1463.e4 (2017).

16. Lim, S. A. O., Kang, U. J. & McGehee, D. S. Striatal cholinergic interneuron regulation and circuit effects. *Front. Synaptic Neurosci.* **6**, 22 (2014).

17. Khakh, B. S. Astrocyte–Neuron Interactions in the Striatum: Insights on Identity, Form, and Function. *Trends Neurosci.* **42**, 617–630 (2019).

18. Kranzler, H. R. Overview of Alcohol Use Disorder. *Am. J. Psychiatry* **180**, 565–572 (2023).

19. The Epidemiology of Drug Abuse - Ignaszewski - 2021 - The Journal of Clinical Pharmacology - Wiley Online Library. https://accp1.onlinelibrary.wiley.com/doi/10.1002/jcph.1937.

20. Koob, G. F. & Volkow, N. D. Neurobiology of addiction: a neurocircuitry analysis. *Lancet Psychiatry* **3**, 760–773 (2016).

21. Everitt, B. J. & Robbins, T. W. Neural systems of reinforcement for drug addiction: from actions to habits to compulsion. *Nat. Neurosci.* **8**, 1481–1489 (2005).

22. Lipton, D. M., Gonzales, B. J. & Citri, A. Dorsal Striatal Circuits for Habits, Compulsions and Addictions. *Front. Syst. Neurosci.* **13**, (2019).

23. Belin, D., Jonkman, S., Dickinson, A., Robbins, T. W. & Everitt, B. J. Parallel and interactive learning processes within the basal ganglia: Relevance for the understanding of addiction. *Behav. Brain Res.* **199**, 89–102 (2009).

24. Lovinger, D. M. & Kash, T. L. Mechanisms of Neuroplasticity and Ethanol's Effects on Plasticity in the Striatum and Bed Nucleus of the Stria Terminalis. *Alcohol Res. Curr. Rev.* **37**, 109–124 (2015).

25. Strong, C. E. & Kabbaj, M. Neural Mechanisms Underlying the Rewarding and Therapeutic Effects of Ketamine as a Treatment for Alcohol Use Disorder. *Front. Behav. Neurosci.* **14**, (2020).

26. Yager, L. M., Garcia, A. F., Donckels, E. A. & Ferguson, S. M. Chemogenetic inhibition of direct pathway striatal neurons normalizes pathological, cue-induced reinstatement of drug-seeking in rats. *Addict. Biol.* **24**, 251–264 (2019).

27. Wang, J. *et al.* Long-lasting adaptations of the NR2B-containing NMDA receptors in the dorsomedial striatum play a crucial role in alcohol consumption and relapse. *J. Neurosci. Off. J. Soc. Neurosci.* **30**, 10187–10198 (2010).

28. Ron, D. & Wang, J. The NMDA Receptor and Alcohol Addiction. in *Biology of the NMDA Receptor* (ed. Van Dongen, A. M.) (CRC Press/Taylor & Francis, Boca Raton (FL), 2009).

29. Wang, J. *et al.* Ethanol-mediated facilitation of AMPA receptor function in the dorsomedial striatum: implications for alcohol drinking behavior. *J. Neurosci. Off. J. Soc. Neurosci.* **32**, 15124–15132 (2012).

30. Choi, S. J. *et al.* Acute inhibition of corticostriatal synaptic transmission in the rat dorsal striatum by ethanol. *Alcohol Fayettev. N* **40**, 95–101 (2006).

31. Haggerty, D. L. *et al.* The role of anterior insular cortex inputs to dorsolateral striatum in binge alcohol drinking. *eLife* **11**, e77411 (2022).

32. DePoy, L. *et al.* Chronic alcohol produces neuroadaptations to prime dorsal striatal learning. *Proc. Natl. Acad. Sci. U. S. A.* **110**, 14783–14788 (2013).

33. Renteria, R. *et al.* Mechanism for differential recruitment of orbitostriatal transmission during actions and outcomes following chronic alcohol exposure. *eLife* **10**, e67065 (2021).

34. Adermark, L., Jonsson, S., Ericson, M. & Söderpalm, B. Intermittent ethanol consumption depresses endocannabinoid-signaling in the dorsolateral striatum of rat. *Neuropharmacology* **61**, 1160–1165 (2011).

35. Jeanblanc, J. *et al.* Endogenous BDNF in the dorsolateral striatum gates alcohol drinking. *J. Neurosci. Off. J. Soc. Neurosci.* **29**, 13494–13502 (2009).

36. Becker, H. C. Effects of Alcohol Dependence and Withdrawal on Stress Responsiveness and Alcohol Consumption. *Alcohol Res. Curr. Rev.* **34**, 448–458 (2012).

37. Blomeley, C. P., Cains, S., Smith, R. & Bracci, E. Ethanol affects striatal interneurons directly and projection neurons through a reduction in cholinergic tone. *Neuropsychopharmacol. Off. Publ. Am. Coll. Neuropsychopharmacol.* **36**, 1033–1046 (2011).

38. Patton, M. H., Roberts, B. M., Lovinger, D. M. & Mathur, B. N. Ethanol Disinhibits Dorsolateral Striatal Medium Spiny Neurons Through Activation of A Presynaptic Delta Opioid Receptor. *Neuropsychopharmacol. Off. Publ. Am. Coll. Neuropsychopharmacol.* **41**, 1831–1840 (2016).

39. Patton, M. S., Sheats, S. H., Siclair, A. N. & Mathur, B. N. Alcohol potentiates multiple GABAergic inputs to dorsal striatum fast-spiking interneurons. *Neuropharmacology* **232**, 109527 (2023).

40. Mews, P. *et al.* Convergent abnormalities in striatal gene networks in human cocaine use disorder and mouse cocaine administration models. *Sci. Adv.* **9**, eadd8946 (2023).

41. Phan, B. N. *et al.* Single nuclei transcriptomics of human and monkey striatum implicates DNA damage, neuroinflammation, and neurodegeneration signaling in opioid use disorder. 2023.05.17.541145 Preprint at https://doi.org/10.1101/2023.05.17.541145 (2023).

42. Brenner, E. *et al.* Single cell transcriptome profiling of the human alcohol-dependent brain. *Hum. Mol. Genet.* **29**, 1144–1153 (2020).

43. Erickson, E. K., Farris, S. P., Blednov, Y. A., Mayfield, R. D. & Harris, R. A. Astrocyte-specific transcriptome responses to chronic ethanol consumption. *Pharmacogenomics J.* **18**, 578–589 (2018).

44. McCarthy, G. M., Farris, S. P., Blednov, Y. A., Harris, R. A. & Mayfield, R. D. Microglial-specific transcriptome changes following chronic alcohol consumption. *Neuropharmacology* **128**, 416–424 (2018).

45. Egervari, G., Siciliano, C. A., Whiteley, E. L. & Ron, D. Alcohol and the brain: from genes to circuits. *Trends Neurosci.* **44**, 1004–1015 (2021).

46. Zillich, L. *et al.* Multi-Omics Signatures of Alcohol Use Disorder in the Dorsal and Ventral Striatum. 2021.10.04.21264523 Preprint at https://doi.org/10.1101/2021.10.04.21264523 (2021).

47. Zhang, L. *et al.* Epigenome-wide meta-analysis of DNA methylation differences in prefrontal cortex implicates the immune processes in Alzheimer's disease. *Nat. Commun.* **11**, 6114 (2020).

48. Lee, J.-M. *et al.* CAG repeat expansion in Huntington disease determines age at onset in a fully dominant fashion. *Neurology* **78**, 690–695 (2012).

49. Ament, S. A. *et al.* High resolution time-course mapping of early transcriptomic, molecular and cellular phenotypes in Huntington's disease CAG knock-in mice across multiple genetic backgrounds. *Hum. Mol. Genet.* **26**, 913–922 (2017).

50. Paulson, H. L. & Albin, R. L. Huntington's Disease: Clinical Features and Routes to Therapy. in *Neurobiology of Huntington's Disease: Applications to Drug Discovery* (eds. Lo, D. C. & Hughes, R. E.) (CRC Press/Taylor & Francis, Boca Raton (FL), 2011).

51. McColgan, P. & Tabrizi, S. J. Huntington's disease: a clinical review. *Eur. J. Neurol.* **25**, 24–34 (2018).

52. Paulsen, J. S. Cognitive Impairment in Huntington Disease: Diagnosis and Treatment. *Curr. Neurol. Neurosci. Rep.* **11**, 474–483 (2011).

53. Horvath, S. *et al.* Huntington's disease accelerates epigenetic aging of human brain and disrupts DNA methylation levels. *Aging* **8**, 1485–1504 (2016).

54. Davis, M. Y., Keene, C. D., Jayadev, S. & Bird, T. The co-occurrence of Alzheimer's disease and Huntington's disease: a neuropathological study of 15 elderly Huntington's disease subjects. *J. Huntingt. Dis.* **3**, 209–217 (2014).

55. 2020 Alzheimer's disease facts and figures. *Alzheimers Dement.* **16**, 391–460 (2020).

56. St-Amour, I., Turgeon, A., Goupil, C., Planel, E. & Hébert, S. S. Co-occurrence of mixed proteinopathies in late-stage Huntington's disease. *Acta Neuropathol. (Berl.)* **135**, 249–265 (2018).

57. Simpson, E. H., Kellendonk, C. & Kandel, E. A Possible Role for the Striatum in the Pathogenesis of the Cognitive Symptoms of Schizophrenia. *Neuron* **65**, 585–596 (2010).

58. Kovalenko, M. *et al.* HttQ111/+ Huntington's Disease Knock-in Mice Exhibit Brain Region-Specific Morphological Changes and Synaptic Dysfunction. *J. Huntingt. Dis.* **7**, 17–33.

59. Lloret, A. *et al.* Genetic background modifies nuclear mutant huntingtin accumulation and HD CAG repeat instability in Huntington's disease knock-in mice. *Hum. Mol. Genet.* **15**, 2015–2024 (2006).

60. Wheeler, V. C. *et al.* Length-dependent gametic CAG repeat instability in the Huntington's disease knock-in mouse. *Hum. Mol. Genet.* **8**, 115–122 (1999).

61. Kaye, J., Reisine, T. & Finkbeiner, S. Huntington's disease mouse models: unraveling the pathology caused by CAG repeat expansion. *Fac. Rev.* **10**, 77 (2021).

62. Rising, A. C. *et al.* Longitudinal behavioral, cross-sectional transcriptional and histopathological characterization of a knock-in mouse model of Huntington's disease with 140 CAG repeats. *Exp. Neurol.* **228**, 173–182 (2011).

63. Dorner, J. L., Miller, B. R., Barton, S. J., Brock, T. J. & Rebec, G. V. Sex differences in behavior and striatal ascorbate release in the 140 CAG knock-in mouse model of Huntington's disease. *Behav. Brain Res.* **178**, 90–97 (2007).

64. Langfelder, P. *et al.* Integrated genomics and proteomics to define huntingtin CAG length-dependent networks in HD Mice. *Nat. Neurosci.* **19**, 623–633 (2016).

65. Lee, H. *et al.* Cell Type-Specific Transcriptomics Reveals that Mutant Huntingtin Leads to Mitochondrial RNA Release and Neuronal Innate Immune Activation. *Neuron* **107**, 891-908.e8 (2020).

66. Malaiya, S. *et al.* Single-nucleus RNA-seq reveals dysregulation of striatal cell identity due to Huntington's disease mutations. *bioRxiv* (2020) doi:10.1101/2020.07.08.192880.

67. Araujo, I., Henriksen, A., Gamsby, J. & Gulick, D. Impact of Alcohol Abuse on Susceptibility to Rare Neurodegenerative Diseases. *Front. Mol. Biosci.* **8**, 643273 (2021).

68. Ehret, J. C., Day, P. S., Wiegand, R., Wojcieszek, J. & Chambers, R. A. Huntington disease as a dual diagnosis disorder: Data from the national research roster

for Huntington disease patients and families. *Drug Alcohol Depend.* **86**, 283–286 (2007).

69. Symonds, A. L., Macerollo, A., Foy, K., Alusi, S. H. & Davies, R. Genetic and Environmental Contributors to Neurodegeneration: An Exploration of the Effects of Alcohol on Clinical Features of Huntington's Disease Using the Enroll-HD Global Platform. *Int. J. Environ. Res. Public. Health* **18**, 5113 (2021).

70. Nogrady, B. How cancer genomics is transforming diagnosis and treatment. *Nature* **579**, S10–S11 (2020).

71. Hill, S. F. & Meisler, M. H. Antisense Oligonucleotide Therapy for Neurodevelopmental Disorders. *Dev. Neurosci.* **43**, 247–252 (2021).

72. Kingwell, K. Double setback for ASO trials in Huntington disease. *Nat. Rev. Drug Discov.* **20**, 412–413 (2021).

73. McColgan, P. *et al.* Tominersen in Adults with Manifest Huntington's Disease. *N. Engl. J. Med.* **389**, 2203–2205 (2023).

74. Understanding Alcohol Use Disorder | National Institute on Alcohol Abuse and Alcoholism (NIAAA). https://www.niaaa.nih.gov/publications/brochures-and-fact-sheets/understanding-alcohol-use-disorder.

75. Patton, M. S., Heckman, M., Kim, C., Mu, C. & Mathur, B. N. Compulsive alcohol consumption is regulated by dorsal striatum fast-spiking interneurons. *Neuropsychopharmacol. Off. Publ. Am. Coll. Neuropsychopharmacol.* **46**, 351–359 (2021).

76. Banerjee, N. Neurotransmitters in alcoholism: A review of neurobiological and genetic studies. *Indian J. Hum. Genet.* **20**, 20–31 (2014).

77. Miller, C. N. & Kamens, H. M. The role of nicotinic acetylcholine receptors in alcohol-related behaviors. *Brain Res. Bull.* **163**, 135–142 (2020).

78. Tupala, E. & Tiihonen, J. Dopamine and alcoholism: neurobiological basis of ethanol abuse. *Prog. Neuropsychopharmacol. Biol. Psychiatry* **28**, 1221–1247 (2004).

79. Sarkisyan, D. *et al.* Downregulation of the endogenous opioid peptides in the dorsal striatum of human alcoholics. *Front. Cell. Neurosci.* **9**, (2015).

80. Clark, S. L. A single-nucleus transcriptomics study of alcohol use disorder in the nucleus accumbens.

81. Becker, H. C. & Lopez, M. F. Increased Ethanol Drinking After Repeated Chronic Ethanol Exposure and Withdrawal Experience in C57BL/6 Mice. *Alcohol. Clin. Exp. Res.* **28**, 1829–1838 (2004).

82. Cortes-Gutierrez, M. *et al.* Frozen Tissue Nuclei Extraction (for 10xV3 snSEQ). (1970).

83. Kamath, T. *et al.* Single-cell genomic profiling of human dopamine neurons identifies a population that selectively degenerates in Parkinson's disease. *Nat. Neurosci.* **25**, 588–595 (2022).

84. Germain, P.-L., Lun, A., Garcia Meixide, C., Macnair, W. & Robinson, M. D. Doublet identification in single-cell sequencing data using scDblFinder. *F1000Research* **10**, 979 (2022).

85. Hao, Y. *et al.* Integrated analysis of multimodal single-cell data. *Cell* **184**, 3573-3587.e29 (2021).

86. Macosko, E. Z. *et al.* Highly Parallel Genome-wide Expression Profiling of Individual Cells Using Nanoliter Droplets. *Cell* **161**, 1202–1214 (2015).

87. Linderman, G. C. *et al.* Zero-preserving imputation of single-cell RNA-seq data. *Nat. Commun.* **13**, 192 (2022).

88. Robinson, M. D., McCarthy, D. J. & Smyth, G. K. edgeR: a Bioconductor package for differential expression analysis of digital gene expression data. *Bioinforma. Oxf. Engl.* **26**, 139–140 (2010).

89. Murphy, A. E. & Skene, N. G. A balanced measure shows superior performance of pseudobulk methods in single-cell RNA-sequencing analysis. *Nat. Commun.* **13**, 7851 (2022).

90. Zhang, Y., Parmigiani, G. & Johnson, W. E. ComBat-seq: batch effect adjustment for RNA-seq count data. *NAR Genomics Bioinforma.* **2**, lqaa078 (2020).

91. limma powers differential expression analyses for RNA-sequencing and microarray studies | Nucleic Acids Research | Oxford Academic. https://academic.oup.com/nar/article/43/7/e47/2414268?ref=https://githubhelp.com.

92. Ament, S. A. *et al.* A single-cell genomic atlas for maturation of the human cerebellum during early childhood. *Sci. Transl. Med.* **15**, eade1283 (2023).

93. Wang, N. *et al.* Mapping brain gene coexpression in daytime transcriptomes unveils diurnal molecular networks and deciphers perturbation gene signatures. *Neuron* **110**, 3318-3338.e9 (2022).

94. Law, C. W., Chen, Y., Shi, W. & Smyth, G. K. voom: Precision weights unlock linear model analysis tools for RNA-seq read counts. *Genome Biol.* **15**, R29 (2014).

95. Lopez, M. F. & Becker, H. C. Effect of pattern and number of chronic ethanol exposures on subsequent voluntary ethanol intake in C57BL/6J mice. *Psychopharmacology (Berl.)* **181**, 688–696 (2005).

96. Griffin, W. C., Lopez, M. F. & Becker, H. C. Intensity and duration of chronic ethanol exposure is critical for subsequent escalation of voluntary ethanol drinking in mice. *Alcohol. Clin. Exp. Res.* **33**, 1893–1900 (2009).

97. Plaisier, S. B., Taschereau, R., Wong, J. A. & Graeber, T. G. Rank–rank hypergeometric overlap: identification of statistically significant overlap between gene-expression signatures. *Nucleic Acids Res.* **38**, e169 (2010).

98. Li, J. *et al.* Chronic Low-Dose Alcohol Consumption Promotes Cerebral Angiogenesis in Mice. *Front. Cardiovasc. Med.* **8**, (2021).

99. Morrow, D., Cullen, J. P., Cahill, P. A. & Redmond, E. M. Ethanol stimulates endothelial cell angiogenic activity via a Notch- and angiopoietin-1-dependent pathway. *Cardiovasc. Res.* **79**, 313–321 (2008).

100. Nakayama, K. & Hasegawa, H. Blood Vessels as a Key Mediator for Ethanol Toxicity: Implication for Neuronal Damage. *Life* **12**, 1882 (2022).

101. Finan, C. *et al.* The druggable genome and support for target identification and validation in drug development. *Sci. Transl. Med.* **9**, eaag1166 (2017).

102. Morales-Garcia, J. A. *et al.* Phosphodiesterase 7 Inhibition Preserves Dopaminergic Neurons in Cellular and Rodent Models of Parkinson Disease. *PLOS ONE* **6**, e17240 (2011).

103. Morales-Garcia, J. A. *et al.* Silencing phosphodiesterase 7B gene by lentiviral-shRNA interference attenuates neurodegeneration and motor deficits in hemiparkinsonian mice. *Neurobiol. Aging* **36**, 1160–1173 (2015).

104. Erro, R., Mencacci, N. E. & Bhatia, K. P. The Emerging Role of Phosphodiesterases in Movement Disorders. *Mov. Disord.* **36**, 2225–2243 (2021).

105. Logrip, M. L. Phosphodiesterase regulation of alcohol drinking in rodents. *Alcohol* **49**, 795–802 (2015).

106. Salinas, A. G. *et al.* Long-term alcohol consumption alters dorsal striatal dopamine release and regulation by D2 dopamine receptors in rhesus macaques. *Neuropsychopharmacology* **46**, 1432–1441 (2021).

107. Trantham-Davidson, H. & Chandler, L. J. Alcohol-induced alterations in dopamine modulation of prefrontal activity. *Alcohol Fayettev. N* **49**, 773–779 (2015).

108. Heinz, A. *et al.* Correlation Between Dopamine D2 Receptors in the Ventral Striatum and Central Processing of Alcohol Cues and Craving. *Am. J. Psychiatry* **161**, 1783–1789 (2004).

109. Feltmann, K. *et al.* Effects of Long-Term Alcohol Drinking on the Dopamine D2 Receptor: Gene Expression and Heteroreceptor Complexes in the Striatum in Rats. *Alcohol. Clin. Exp. Res.* **42**, 338–351 (2018).

110. Hamada, K. & Lasek, A. W. Receptor Tyrosine Kinases as Therapeutic Targets for Alcohol Use Disorder. *Neurotherapeutics* **17**, 4–16 (2020).

111. Deinhardt, K. & Chao, M. V. Trk Receptors. in *Neurotrophic Factors* (eds. Lewin, G. R. & Carter, B. D.) 103–119 (Springer, Berlin, Heidelberg, 2014). doi:10.1007/978-3-642-45106-5_5.

112. Gupta, V. K., You, Y., Gupta, V. B., Klistorner, A. & Graham, S. L. TrkB Receptor Signalling: Implications in Neurodegenerative, Psychiatric and Proliferative Disorders. *Int. J. Mol. Sci.* **14**, 10122–10142 (2013).

113. Altar, C. A. *et al.* Anterograde transport of brain-derived neurotrophic factor and its role in the brain. *Nature* **389**, 856–860 (1997).

114. Li, Y. *et al.* Conditional ablation of brain-derived neurotrophic factor-TrkB signaling impairs striatal neuron development. *Proc. Natl. Acad. Sci.* **109**, 15491–15496 (2012).

115. Logrip, M. L., Barak, S., Warnault, V. & Ron, D. Corticostriatal BDNF and alcohol addiction. *Brain Res.* **1628**, 60–67 (2015).

116. Ghezzi, P., Bigini, P. & Mengozzi, M. Role of Erythropoietin in Inflammatory Pathologies of the CNS. in *Erythropoietin and the Nervous System: Novel Therapeutic Options for Neuroprotection* (ed. Höke, A.) 191–209 (Springer US, Boston, MA, 2006). doi:10.1007/978-0-387-30011-5_12.

117. Rey, F. *et al.* Erythropoietin as a Neuroprotective Molecule: An Overview of Its Therapeutic Potential in Neurodegenerative Diseases. *ASN Neuro* **11**, 1759091419871420 (2019).

118. Hendriks, J. J. A. *et al.* Leukemia inhibitory factor modulates production of inflammatory mediators and myelin phagocytosis by macrophages. *J. Neuroimmunol.* **204**, 52–57 (2008).

119. Luo, Y. *et al.* EPO prevents neuroinflammation and relieves depression via JAK/STAT signaling. *Life Sci.* **333**, 122102 (2023).

120. Kim, H. *et al.* AIM2 inflammasome contributes to brain injury and chronic post-stroke cognitive impairment in mice. *Brain. Behav. Immun.* **87**, 765–776 (2020).

121. Chai, L. *et al.* LRRC19, a novel member of the leucine-rich repeat protein family, activates NF-κB and induces expression of proinflammatory cytokines. *Biochem. Biophys. Res. Commun.* **388**, 543–548 (2009).

122. Lima, I. V. de A., Bastos, L. F. S., Limborço-Filho, M., Fiebich, B. L. & de Oliveira, A. C. P. Role of Prostaglandins in Neuroinflammatory and Neurodegenerative Diseases. *Mediators Inflamm.* **2012**, 946813 (2012).

123. Bordon, Y. Fine-tuning of inflammation by F-box proteins. *Nat. Rev. Immunol.* **13**, 305–305 (2013).

124. Na, Y. R. *et al.* Prostaglandin E2 receptor PTGER4-expressing macrophages promote intestinal epithelial barrier regeneration upon inflammation. *Gut* **70**, 2249–2260 (2021).

125. Heger, K. *et al.* OTULIN limits cell death and inflammation by deubiquitinating LUBAC. *Nature* **559**, 120–124 (2018).

126. Ren, Y. *et al.* Spata2 Knockdown Exacerbates Brain Inflammation via NF-κB/P38MAPK Signaling and NLRP3 Inflammasome Activation in Cerebral Ischemia/Reperfusion Rats. *Neurochem. Res.* **46**, 2262–2275 (2021).

127. Cardamone, M. D. *et al.* A Protective Strategy against Hyperinflammatory Responses Requiring the Nontranscriptional Actions of GPS2. *Mol. Cell* **46**, 91–104 (2012).

128. Achur, R. N., Freeman, W. M. & Vrana, K. E. Circulating Cytokines as Biomarkers of Alcohol Abuse and Alcoholism. *J. Neuroimmune Pharmacol. Off. J. Soc. NeuroImmune Pharmacol.* **5**, 83–91 (2010).

129. Adams, C. *et al.* Central markers of neuroinflammation in alcohol use disorder: A meta-analysis of neuroimaging, cerebral spinal fluid, and postmortem studies. *Alcohol Clin. Exp. Res.* **47**, 197–208 (2023).

130. Erickson, E. K., Grantham, E. K., Warden, A. S. & Harris, R. A. Neuroimmune signaling in alcohol use disorder. *Pharmacol. Biochem. Behav.* **177**, 34–60 (2019).

131. Lékó, A. H., Ray, L. A. & Leggio, L. The vicious cycle between (neuro)inflammation and alcohol use disorder: An opportunity to develop new medications? *Alcohol Clin. Exp. Res.* **47**, 843–847 (2023).

132. Crews, F. T., Lawrimore, C. J., Walter, T. J. & Coleman, L. G. The role of neuroimmune signaling in alcoholism. *Neuropharmacology* **122**, 56–73 (2017).

133. Kitagawa, M. *et al.* Hes1 and Hes5 regulate vascular remodeling and arterial specification of endothelial cells in brain vascular development. *Mech. Dev.* **130**, 458–466 (2013).

134. Hes1 and Hes5 as Notch effectors in mammalian neuronal differentiation. https://www.embopress.org/doi/epdf/10.1093/emboj/18.8.2196?src=getftr doi:10.1093/emboj/18.8.2196.

135. Liu, Z.-J. *et al.* Inhibition of endothelial cell proliferation by Notch1 signaling is mediated by repressing MAPK and PI3K/Akt pathways and requires MAML1. *FASEB J. Off. Publ. Fed. Am. Soc. Exp. Biol.* **20**, 1009–1011 (2006).

136. Quillard, T. *et al.* Impaired Notch4 Activity Elicits Endothelial Cell Activation and Apoptosis. *Arterioscler. Thromb. Vasc. Biol.* **28**, 2258–2265 (2008).

137. Lebrin, F., Deckers, M., Bertolino, P. & ten Dijke, P. TGF-β receptor function in the endothelium. *Cardiovasc. Res.* **65**, 599–608 (2005).

138. Jarad, M., Kuczynski, E. A., Morrison, J., Viloria-Petit, A. M. & Coomber, B. L. Release of endothelial cell associated VEGFR2 during TGF-β modulated angiogenesis in vitro. *BMC Cell Biol.* **18**, 10 (2017).

139. Solár, P., Zamani, A., Kubíčková, L., Dubový, P. & Joukal, M. Choroid plexus and the blood–cerebrospinal fluid barrier in disease. *Fluids Barriers CNS* **17**, 35 (2020).

140. Day, S. M. *et al.* Ethanol exposure alters Alzheimer's-related pathology, behavior, and metabolism in APP/PS1 mice. *Neurobiol. Dis.* **177**, 105967 (2023).

141. Gong, Y.-S., Hou, F.-L., Guo, J., Lin, L. & Zhu, F.-Y. Effects of alcohol intake on cognitive function and β-amyloid protein in APP/PS1 transgenic mice. *Food Chem. Toxicol.* **151**, 112105 (2021).

142. Gião, T. *et al.* Neuroprotection in early stages of Alzheimer's disease is promoted by transthyretin angiogenic properties. *Alzheimers Res. Ther.* **13**, 143 (2021).

143. Shao, J. *et al.* Transthyretin Exerts Pro-Apoptotic Effects in Human Retinal Microvascular Endothelial Cells Through a GRP78-Dependent Pathway in Diabetic Retinopathy. *Cell. Physiol. Biochem.* **43**, 788–800 (2017).

144. Vore, A. S. & Deak, T. Alcohol, Inflammation, and Blood-Brain Barrier Function in Health and Disease Across Development. *Int. Rev. Neurobiol.* **161**, 209–249 (2022).

145. Carrino, D. *et al.* Alcohol-Induced Blood-Brain Barrier Impairment: An In Vitro Study. *Int. J. Environ. Res. Public. Health* **18**, 2683 (2021).

146. Logrip, M. L., Vendruscolo, L. F., Schlosburg, J. E., Koob, G. F. & Zorrilla, E. P. Phosphodiesterase 10A regulates alcohol and saccharin self-administration in rats. *Neuropsychopharmacol. Off. Publ. Am. Coll. Neuropsychopharmacol.* **39**, 1722–1731 (2014).

147. Menniti, F. S., Chappie, T. A. & Schmidt, C. J. PDE10A Inhibitors-Clinical Failure or Window Into Antipsychotic Drug Action? *Front. Neurosci.* **14**, 600178 (2020).

148. Cuzon Carlson, V. C. *et al.* Synaptic and morphological neuroadaptations in the putamen associated with long-term, relapsing alcohol drinking in primates. *Neuropsychopharmacol. Off. Publ. Am. Coll. Neuropsychopharmacol.* **36**, 2513–2528 (2011).

149. Wilcox, M. V. *et al.* Repeated binge-like ethanol drinking alters ethanol drinking patterns and depresses striatal GABAergic transmission. *Neuropsychopharmacol. Off. Publ. Am. Coll. Neuropsychopharmacol.* **39**, 579–594 (2014).

150. Cuzon Carlson, V. C., Grant, K. A. & Lovinger, D. M. Synaptic adaptations to chronic ethanol intake in male rhesus monkey dorsal striatum depend on age of drinking onset. *Neuropharmacology* **131**, 128–142 (2018).

151. Han, I., You, Y., Kordower, J. H., Brady, S. T. & Morfini, G. A. Differential vulnerability of neurons in Huntington's disease: The role of cell type-specific features. *J. Neurochem.* **113**, 1073–1091 (2010).

152. Walker, F. O. Huntington's disease. *Lancet Lond. Engl.* **369**, 218–228 (2007).

153. Pandey, M. & Rajamma, U. Huntington's disease: the coming of age. *J. Genet.* **97**, 649–664 (2018).

154. Kim, A. *et al.* New Avenues for the Treatment of Huntington's Disease. *Int. J. Mol. Sci.* **22**, 8363 (2021).

155. Details emerge on tominersen trial halt. https://www.cureffi.org/2021/04/28/details-tominersen-trial-halt/.

156. Tominersen being rebooted for early HD. https://www.cureffi.org/2022/01/21/tominersen-rebooted/.

157. Hodges, A. *et al.* Regional and cellular gene expression changes in human Huntington's disease brain. *Hum. Mol. Genet.* **15**, 965–977 (2006).

158. Malaiya, S. *et al.* Single-nucleus RNA-seq reveals dysregulation of striatal cell identity due to Huntington's disease mutations. *bioRxiv* 2020.07.08.192880 (2020) doi:10.1101/2020.07.08.192880.

159. Zamanian, J. L. *et al.* Genomic analysis of reactive astrogliosis. *J. Neurosci. Off. J. Soc. Neurosci.* **32**, 6391–6410 (2012).

160. Russell, D. S. *et al.* Change in PDE10 across early Huntington disease assessed by [18F]MNI-659 and PET imaging. *Neurology* **86**, 748–754 (2016).

161. Stefanko, D. P., Shah, V. D., Yamasaki, W. K., Petzinger, G. M. & Jakowec, M. W. Treadmill exercise delays the onset of non-motor behaviors and striatal pathology in the CAG140 knock-in mouse model of Huntington's disease. *Neurobiol. Dis.* **105**, 15–32 (2017).

162. Reiner, A. & Deng, Y. Disrupted striatal neuron inputs and outputs in Huntington's disease. *CNS Neurosci. Ther.* **24**, 250–280 (2018).

163. Deng, Y., Wang, H., Joni, M., Sekhri, R. & Reiner, A. Progression of basal ganglia pathology in heterozygous Q175 knock-in Huntington's disease mice. *J. Comp. Neurol.* **529**, 1327–1371 (2021).

164. Linville, R. M. *et al.* Brain microvascular endothelial cell dysfunction in an isogenic juvenile iPSC model of Huntington's disease. *Fluids Barriers CNS* **19**, 54 (2022).

165. Padel, T. *et al.* Brain pericyte activation occurs early in Huntington's disease. *Exp. Neurol.* **305**, 139–150 (2018).

166. Wilton, D. K. & Stevens, B. The contribution of glial cells to Huntington's disease pathogenesis. *Neurobiol. Dis.* **143**, 104963 (2020).

167. Mockus, T. E. *et al.* CD8 T Cells and STAT1 Signaling Are Essential Codeterminants in Protection from Polyomavirus Encephalopathy. *J. Virol.* **94**, e02038-19 (2020).

168. Nelles, D. G. & Hazrati, L.-N. Ependymal cells and neurodegenerative disease: outcomes of compromised ependymal barrier function. *Brain Commun.* **4**, fcac288 (2022).

169. Keryer, G. *et al.* Ciliogenesis is regulated by a huntingtin-HAP1-PCM1 pathway and is altered in Huntington disease. *J. Clin. Invest.* **121**, 4372–4382 (2011).

170. Dietrich, P., Shanmugasundaram, R., Shuyu, E. & Dragatsis, I. Congenital hydrocephalus associated with abnormal subcommissural organ in mice lacking huntingtin in Wnt1 cell lineages. *Hum. Mol. Genet.* **18**, 142–150 (2009).

171. Tang, B. H., Lieberman, A. & Rovit, R. Huntington's chorea associated with normal pressure hydrocephalus. *Eur. Neurol.* **13**, 189–194 (1975).

172. Shirani, P., Salamone, A. R., Lahijani, E., York, M. K. & Schulz, P. E. Lumbar puncture alleviates chorea in a patient with Huntington's disease and normal pressure hydrocephalus. *Behav. Neurol.* **21**, 193–195 (2009).

173. Caserta, M. T. & Sullivan, E. Late-Onset Huntington's Disease Masquerading as Normal Pressure Hydrocephalus. *J. Neuropsychiatry Clin. Neurosci.* **21**, 97–98 (2009).

174. Stoker, T. B., Andresen, K. E. R. & Barker, R. A. Hydrocephalus Complicating Intrathecal Antisense Oligonucleotide Therapy for Huntington's Disease. *Mov. Disord.* **36**, 263–264 (2021).

175. Oliver, C. *et al.* Disruption of CDH2/N-Cadherin-Based Adherens Junctions Leads to Apoptosis of Ependymal Cells and Denudation of Brain Ventricular Walls. *J. Neuropathol. Exp. Neurol.* **72**, 846–860 (2013).

176. Serra, R. & Simard, J. M. Adherens, tight, and gap junctions in ependymal cells: A systematic review of their contribution to CSF-brain barrier. *Front. Neurol.* **14**, (2023).

177. Southwell, A. L. *et al.* Huntingtin suppression restores cognitive function in a mouse model of Huntington's disease. *Sci. Transl. Med.* **10**, eaar3959 (2018).

178. Southwell, A. L. *et al.* Huntingtin suppression restores cognitive function in a mouse model of Huntington's disease. *Sci. Transl. Med.* **10**, eaar3959 (2018).